Elie A. Shammas
Howie Choset
Alfred A. Rizzi

The Robotics Institute, Carnegie Mellon University
5000 Forbes Avenue, Pittsburgh, PA 15213, USA
choset@ri.cmu.edu

Geometric Motion Planning Analysis for Two Classes of Underactuated Mechanical Systems

Abstract

In this paper we generate gaits for two types of underactuated mechanical systems: principally kinematic and purely mechanical systems. Our goal is to specify inputs in the form of gaits, that is, a sequence of controlled shape changes of a multi-bodied mechanical system that when executed would produce a desired change in the unactuated position or orientation variables of the entire mechanical system. In other words, we want to indirectly control the unactuated degrees of freedom of the mechanical system utilizing a controlled "internal" shape change. More precisely, in this paper we develop a gait evaluation tool which easily measures the change of position, computed in a body-attached coordinate frame, due to any closed curve in the shape space. This evaluation tool is simple enough that we can use it to generate gaits or to design curves that move the mechanical system along a desired direction. Finally, we verify that this gait analysis technique applies to two seemingly different classes of mechanical systems, purely mechanical and principally kinematic systems, and unify the gait generation problem for both classes.

KEY WORDS—gait generation, motion control, underactuated robots, non-holonomic motion planning, generalized momentum, purely mechanical systems, principally kinematic systems, Stokes' theorem

1. Introduction

In this paper we develop a general and intuitive formulation of the gait analysis and generation problem that applies to two classes of mechanical systems. We actually classify mechanical systems into three categories: *purely mechanical systems*, that is, systems whose motion is governed solely by the conservation of momentum; *principally kinematic systems*, that is, systems whose motion is governed solely by the existence of a set of independent non-holonomic velocity constraints that fully specify the systems' motion; and *dynamic systems with non-holonomic constraints*, that is, systems whose motion is governed by a non-holonomic set of constraints and generalized momentum being constrained by a set of differential equations.

In this paper we develop motion analysis and planning techniques for the first two types of mechanical system, the purely mechanical and principally kinematic systems. We demonstrate our techniques using two example systems: the *pivoting dynamic robot*, shown in Figure 1, which is a purely mechanical system; and the *kinematic snake robot*, shown in Figure 2, which is a principally kinematic system. We extend the results presented in this paper to generate gaits for the third type of mechanical systems, the more general family of dynamic systems with non-holonomic constraints, in a companion paper (Shammas et al. 2007).

Recall that the *configuration space* of mechanical systems can be naturally divided into two subspaces: the *fiber space*, which represents the position of the system with respect to a fixed inertial frame; and the *base space*, which represents the internal degrees of freedom of the robot, that is, the robot's shape. As we assume control solely over the base variables, the mechanical systems we consider are necessarily *underactuated*. We generate gaits for both the pivoting dynamic model and the kinematic snake robot to move them along a specified fiber direction solely by coordinating their two inter-link angles, that is, their base variables.

What is interesting about purely mechanical and principally kinematic systems is that, even though the motions of these two systems are derived from two different governing laws,

The International Journal of Robotics Research
Vol. 26, No. 10, October 2007, pp. 1043–1073
DOI: 10.1177/0278364907082106
©SAGE Publications 2007 Los Angeles, London, New Delhi and Singapore
Figures 2–4, 6–19 appear in color online: http://ijr.sagepub.com

Downloaded from ijr.sagepub.com at PENNSYLVANIA STATE UNIV on May 16, 2016

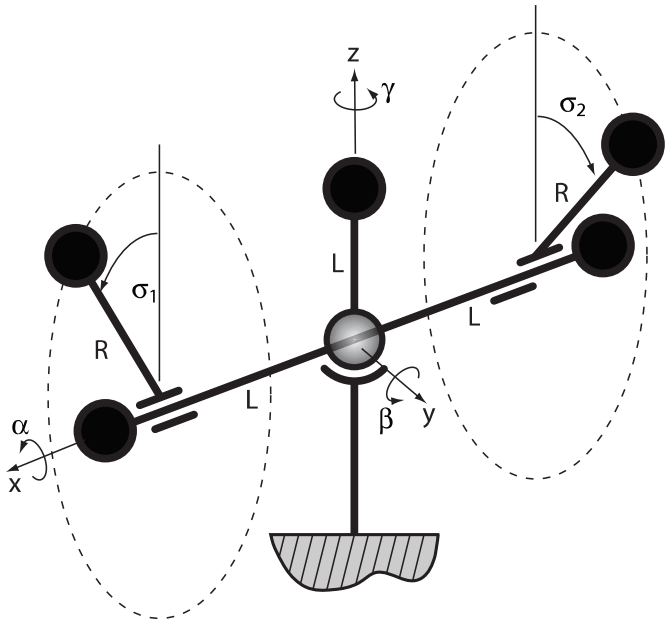

Fig. 1. A schematic of the *pivoting dynamic model* denoting its five configuration variables, $(\alpha, \beta, \gamma, \sigma_1, \sigma_2)$. After verifying that the system's motion is solely governed by the law of momentum conservation and proving that it is a purely mechanical system, we generate gaits by specifying how to actuate the angles of the left and right arms, represented by the base variables (σ_1, σ_2), so that the system will change its orientation, represented by the fiber variables (α, β, γ).

the fiber motion of both systems can be "directly" related to their base motions with a structurally identical relation. We show later in the paper how to derive this relationship for both classes of systems. The similarity of this relation allows us to design gaits for both systems using the same technique.

We have chosen the pivoting dynamic model and the kinematic snake robot to demonstrate our gait analysis techniques because these systems strike a balance between being similar enough to previous work to allow a comparison of our method with prior techniques and being complex enough that one cannot simply make any intuitive guesses about generating gaits. Moreover, analyzing these relatively general examples allows us to verify the utility and applicability of our gait analysis techniques.

2. Prior Work

Gait generation, the problem of designing curves in the base space that induce a desired position change, has been extensively studied in the literature. We build upon and seek to unify and generalize the prior work results in gait analysis and generation.

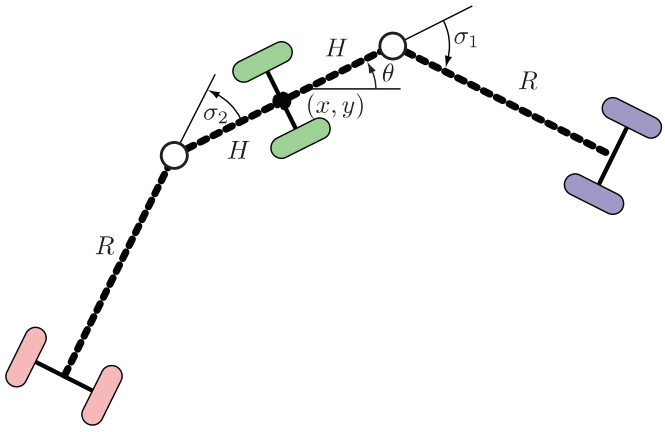

Fig. 2. A schematic of the *kinematic snake robot* denoting its five configuration variables, $(x, y, \theta, \sigma_1, \sigma_2)$. After verifying that the system's motion is solely governed by a set of nonholonomic velocity constraints and proving that it is a principally kinematic system, we generate gaits by specifying how to actuate the inter-link angles, represented by the base variables (σ_1, σ_2), so that the system will change its position and orientation, represented by the fiber variables (x, y, θ).

2.1. Bio-mimetic Approach

Hirose (1993) took a bio-mimetic approach to develop locomoting robotic snakes. By performing extensive experiments on biological snakes to study how they locomote, he constructed robotic snakes that moved by mimicking their biological counterparts. He was able to define a geometric curve, the *serpenoid* curve, which approximates the shape of a real snake during undulation. Moreover, Hirose designed and built several robotic snakes which were composed of numerous rigid links that were connected by revolute joints. By attaching passive wheels on the bottom of the links and forcing the robot's shape to move along the serpenoid curve, Hirose demonstrated robotic snake locomotion, similar to biological snake locomotion, on planar serially linked robots.

In fact, the second example system we are analyzing in this paper, the kinematic snake, is a simplified version of the snake robots constructed and analyzed by Hirose. We shall see how our simplif ied system with only a two-dimensional base space has enough actuation to fully span the fiber space, that is, translate and orient the snake-like robot in the plane.

2.2. Sinusoidal Inputs Approach

Originally, sinusoidal inputs were motivated by Brockett and Dai's work on the controllability of mechanical systems (Brockett 1981; Brockett and Dai 1993). They derived optimal sinusoidal inputs for a set of canonical systems for which

Downloaded from ijr.sagepub.com at PENNSYLVANIA STATE UNIV on May 16, 2016

the tangent space is spanned by the input vector fields as well as the *first-order* Lie brackets of the input vector fields. Murray and Sastry (1993) derived suboptimal inputs for mechanical systems where the tangent space is spanned by the input vector fields and more than first-order Lie brackets.

In addition, several researchers have assumed that the base inputs of the mechanical systems are sinusoidal, hence, simplifying the controllability analysis as well as the gait generation problem. For example, Murray and Sastry (1993) and Walsh and Sastry (1991, 1995) studied the dynamics of a planar three-link robot floating in space. By writing the Lagrangian of the system in a special form, they were able to generate gaits for the planar three-link snake robot. They have proposed *sinusoidal* gaits and then computed the *geometric* phase shift produced by these gaits. It is worth noting that the pivoting dynamic model that we are analyzing in this paper is a spatial version of the system considered by Walsh and Sastry (1991, 1995).

Ostrowski and Burdick (1998) and Ostrowski et al. (2000), on the other hand, took a more fundamental approach and generalized Walsh's approach by taking advantage of the idea of translational symmetry from physics. This allowed them to project the entire dynamics of the system onto the base space. Moreover, by representing the system dynamics with respect to a body-fixed coordinate frame, a relation between fiber velocity, on the one hand, and base and momentum variables, on the other, was devised. This decoupling relation is referred to as the *reconstruction equation* which allowed the system's dynamics to be represented as an affine non-linear control system. Then, by taking recourse to geometric control theory, the degree of Lie brackets of the control vector fields required to span the fiber velocities was related to the frequencies of the sinusoidal inputs of the base variables (Ostrowski and Burdick 1998; Ostrowski et al. 2000). Using this approach, they intuitively developed and then analyzed gaits for principally kinematic and dynamic systems with non-holonomic constraints. This approach was applicable to *sinusoidal* inputs where only the gait frequencies were determined, however, the magnitudes were empirically derived to produce the desired motion. For further involved reading on the topics of non-holonomic mechanics and symmetry, the reader is referred to Bloch et al. (2003, Chapters 1–5) and Marsden and Ratiu (1994, Chapters 4, 7 and 9), respectively.

Again, one of the systems that was analyzed by Ostrowski and Burdick (1998) is almost identical to the kinematic snake example we are analyzing in this paper. The main difference is that our version has a two-dimensional base space whereas Ostrowski's version had a five-dimensional base space.

Finally, we would like to mention the work of Chitta et al. (2004, 2005) who developed several unconventional locomoting robots, such as the rollerblader and the robo-Trikke. They have used Ostrowski's techniques to generate sinusoidal gaits for these novel locomoting robots.

Table 1. Dimensions of various vectors and matrices.

Matrix	Dimension	Description
g, ξ	$l \times 1$	Fiber variables, body velocity
r	$m \times 1$	Base variables
q	$n \times 1$	Configuration variables
M	$n \times n$	Mass matrix
A	$l \times m$	Local connection form
I	$l \times l$	Locked inertia tensor
p	$1 \times (l-k)$	Generalized non-holonomic momentum
ω	$k \times n$	Pfaffian constraint matrix
λ	$k \times 1$	Constraint forces

2.3. Integration Approach

The main idea of this approach is to relate position changes to volume integrals under well-defined functions. Using this approach, Nakamura and Mukherjee (1989, 1991) and Mukherjee and Anderson (1993) generated gaits for the rolling disk which is a principally kinematic system. In fact, they generated gaits that produced a desired motion with a specified magnitude for only the particular example of the rolling disk. This task was done by limiting the gaits to closed rectangular curves, thus solving the volume integrals analytically. This is not the case in general, and for more general systems position change in a body-attached coordinate frame is not directly related to the global position change of the mechanical system.

Finally, it is worth mentioning that there has been other prior work that directly relates to the integration approach. Yamada (1993) was concerned with purely mechanical systems and he generated gaits only for space robots. We developed a similar but more general approach and generated gaits for two types of mechanical systems: purely mechanical systems in Shammas et al. (2005b) and principally kinematic systems in Shammas et al. (2005a).

3. Background Material

In this section we very briefly review some basic ideas and concepts from Lagrangian mechanics and mechanics of locomotion. An extended and detailed version of this section can be found in Appendix A.

The configuration space of mechanical systems is usually denoted by Q and it has a trivial fiber bundle structure. That is, $Q = G \times M$, where G is the fiber space with a Lie group structure that represents the position of the robot with respect to an inertial coordinate frame and M is the base space which represents the internal degrees of freedom of the system. Thus,

Downloaded from ijr.sagepub.com at PENNSYLVANIA STATE UNIV on May 16, 2016

a configuration variable can be written as $q = (g, r) \in Q$ where g is the fiber variable and r is the base variable. A configuration velocity is denoted as $\dot{q} = (\dot{g}, \dot{r}) \in T_q Q$, the tangent space of the manifold Q at the configuration q.

For a mechanical system we can define the Lagrangian, $L(q, \dot{q})$, which is a map from the tangent space of the configuration manifold to the reals. For mechanical systems, the Lagrangian is usually defined as the kinetic energy of the system minus its potential energy, however, in this paper, we neglect any potential energy and equate the Lagrangian to the system's kinetic energy, that is,

$$L(q, \dot{q}) = \tfrac{1}{2}\dot{q}^{\mathrm{T}} M(q)\dot{q}, \tag{1}$$

where $M(q)$ is the mass matrix. Moreover, in this paper we deal with non-holonomic constraints, which are velocity constraints that are by definition not integrable. We assume that we can always write the set of k non-holonomic constraints in the following Pfaffian form

$$\omega(q) \cdot \dot{q} = 0, \tag{2}$$

where $\omega(q)$ is a $k \times n$ matrix describing the constraints. For this paper, we utilize the triviality of the configuration space to partition the matrix $\omega(q)$ and rewrite (2) as

$$\omega_g(q) \cdot \dot{g} + \omega_r(q) \cdot \dot{r} = 0, \tag{3}$$

where $\omega_g(q)$ and $\omega_r(q)$ are sub-matrices of $\omega(q)$.

Hence, for a mechanical system with a set of non-holonomic constraints, we can write the system's equations of motion, or the Euler–Lagrange equations, as

$$\frac{d}{dt}\left(\frac{\partial L(q, \dot{q})}{\partial \dot{q}_i}\right) - \frac{\partial L(q, \dot{q})}{\partial q_i} + \lambda_j \omega_i^j(q) = \tau_i, \tag{4}$$

for all $i = 1, \ldots, n$, where n is the dimension of Q, $j = 1, \ldots, k$, where k is the number of non-holonomic constraints acting on the mechanical system, λ are the Lagrange multipliers and τ_i are the generalized forces.

Moreover, we can exploit the symmetries in the laws of physics to reduce the order of the above dynamic equations of motion. This reduction process is possible when one can prove the independence of the system dynamics with respect to the fiber configuration variables as well as by means of a rewriting the equations of motion in terms of a generalized momentum variable.

Before we can rewrite the equations of motion in a reduced form, we need to define actions and lifted actions that arise from the Lie group structure of the fiber space. The group action denoted by Φ_h is used to map a configuration $q = (g, r)$ to another configuration $\Phi_h q = (L_h g, r)$, where L_h is the left translation of the Lie group. Similarly we can define the lifted left action on the group which is a linear map that maps configuration velocities or elements of the tangent space. The lifted action is usually denoted by $T_q \Phi_h \dot{q}$ which maps a velocity $\dot{q} = (\dot{g}, \dot{r})$ to another velocity $(T_g L_h \dot{g}, \dot{r})$. Then using these actions we map the system dynamics to the Lie group identity, $g = e$, and define the reduced Lagrangian which will have the following structure

$$l(\xi, r, \dot{r}) = \frac{1}{2}\begin{pmatrix}\xi & \dot{r}\end{pmatrix}^{\mathrm{T}} \tilde{M} \begin{pmatrix}\xi \\ \dot{r}\end{pmatrix} \tag{5}$$

where

$$\tilde{M} = \begin{pmatrix} I(r) & I(r)A(r) \\ A^{\mathrm{T}}(r) I^{\mathrm{T}}(r) & m(r) \end{pmatrix}. \tag{6}$$

Here $\tilde{M}$ is the reduced mass matrix, $A(r)$ is the local form of the mechanical connection, $I(r)$ is the local form of the locked inertia tensor, $m(r)$ is an $m \times m$ matrix that depends only on the base variables and ξ is a body representation of a fiber velocity $\dot{g}$, that is,

$$\xi = T_g L_g^{-1} \dot{g}. \tag{7}$$

Note that $A(r)$ and $I(r)$, the respective local forms of the mechanical connection, $\mathcal{A}(q)$, and the locked inertia tensor, $\mathbb{I}(q)$, arise due to the triviality of the fiber bundle as shown in Appendix A.

Similarly, we can rewrite the non-holonomic constraints in a body-attached coordinate frame to obtain

$$\bar{\omega}_\xi(r)\xi + \bar{\omega}_r(r)\dot{r} = 0, \tag{8}$$

where $\bar{\omega}_\xi(r)$ and $\bar{\omega}_r(r)$ are computed from (3) by setting $g = e$ and substituting for $\dot{g}$ using (7) as we prove in Lemma B.1 in Appendix B.

Now, before we rewrite the dynamic equations of motion in their reduced form, we take recourse to the mechanics of locomotion to define the generalized momentum, $p = \frac{\partial l}{\partial \xi}$; moreover, utilizing the triviality of the configuration space of mechanical systems, we can relate the group velocity expressed in a body-attached coordinate frame by the following equation

$$\xi = T_g L_{g^{-1}} \dot{g} = -A(r)\dot{r} + I^{-1}(r) p^{\mathrm{T}}, \tag{9}$$

where $A(r)$ is the local form of the mechanical connection and $I(r)$ is the local form of the locked inertia tensor. Equation (9) is referred to as the *reconstruction* equation, because it can be utilized to reconstruct the group variables, g, for a given momentum and base configuration and velocity variables, p and $(r, \dot{r})$, respectively. We derive this equation in Appendix A.

Now we are ready to write the dynamic equations of motion in their reduced form so that we can compute the momentum and base variables. Thus, the dynamic equations of motion (4) for unconstrained mechanical systems become

$$\dot{p}_i - \mathrm{ad}^*_\xi p_i = \tau_i^e \tag{10}$$

$$\frac{d}{dt}\left(\frac{\partial l}{\partial \dot{r}^j}\right) - \frac{\partial l}{\partial r^j} = \tau_j^r \tag{11}$$

Downloaded from ijr.sagepub.com at PENNSYLVANIA STATE UNIV on May 16, 2016

where for $i = 1, \ldots, l$, τ_i^e are the forcing functions in the group directions pulled back to the group identity (for the reduced form of the Lagrangian) and, for $j = 1, \ldots, m$, τ_j^r are the base forcing functions. The first equation represents the momentum evolution equation with the momentum, p, and the second equation constitutes the dynamic equations for the base space.

Finally, note that we used invariance to represent the n second-order dynamic equations of the mechanical system shown in (4) to a reduced first-order set of $2l$ equations and a smaller set of m second-order equations shown in (9)–(11). Refer to the Appendix A for more details.

4. Examples

Throughout this paper, we use two example systems to demonstrate our ideas and eventually generate gaits for these two systems. We start by introducing these two example systems, then we define their conf iguration spaces, compute their reduced Lagrangians and write their set of non-holonomic constraints in body coordinates.

Example 1: Pivoting Dynamic Model

The *pivoting dynamic model* was first introduced by Balasubramanian and Rizzi (2004) and Balasubramanian et al. (2003) as a novel locomoting system. The pivoting dynamic model shown in Figure 1 is composed of three rigid links. The outer two links are connected to the middle link by means of two revolute joints whose axes are coincident with the middle link. Thus, the outer two links will always lie in two parallel planes that are perpendicular to the middle link. The outer two links have mass concentrated at their distal ends, while the middle link has three concentrated masses at each of its distal ends and one in the middle. The middle link is connected to the ground by manes of a spherical joint at the link center.

We attach a body coordinate frame to the middle of the center link as shown in Figure 1. The orientation of this body frame is represented by the three fiber variables, (α, β, γ), which denote three rotations along the three frame axes. The two internal degrees of freedom are represented by the relative angle between the links (σ_1, σ_2). Note that the axis of rotation of the two distal links are aligned along the middle link.

Hence, the pivoting dynamic model has a five-dimensional, $(n = 5)$, configuration space $Q = G \times M$, where the associated Lie group fiber space $G = \mathrm{SO}(3)$, the three-dimensional special orthogonal group, denotes the robot's orientation. The base space denoting the internal degrees of freedom is $M = \mathbb{S} \times \mathbb{S}$. The Lagrangian of the pivoting dynamic model in the absence of gravity is

$$L(q, \dot{q}) = \frac{1}{2} \sum_{i=1}^{5} (m_i \dot{x}_i^{\mathrm{T}} \dot{x}_i), \tag{12}$$

where m_i represents the mass of each of the concentrated masses and each x_i represents the inertial position of these masses. Let the length of the middle link be $2H$ while the length of the outer links be R. To simplify some expressions we will assume that all the mass are identical, that is, $m_i = m$.

We define the rotation matrices about the three axes in the usual way, that is,

$$R_x(\alpha) = \begin{pmatrix} 1 & 0 & 0 \\ 0 & \cos(\alpha) & -\sin(\alpha) \\ 0 & \sin(\alpha) & \cos(\alpha) \end{pmatrix},$$

$$R_y(\beta) = \begin{pmatrix} \cos(\beta) & 0 & \sin(\beta) \\ 0 & 1 & 0 \\ -\sin(\beta) & 0 & \cos(\beta) \end{pmatrix},$$

and

$$R_z(\gamma) = \begin{pmatrix} \cos(\gamma) & -\sin(\gamma) & 0 \\ \sin(\gamma) & \cos(\gamma) & 0 \\ 0 & 0 & 1 \end{pmatrix}.$$

Given that the fiber space has an SO(3) group structure, we define the group action as $L_g = R_z(\gamma) R_y(\beta) R_x(\alpha)$. Since $L_g \in \mathrm{SO}(3)$, we can compute the lifted action as defined in Murray et al. (1994, Chapter 2), where

$$T_g L_{g^{-1}} = (L_g)^{\mathrm{T}} \frac{d}{dt}(L_g).$$

Then we can compute the lifted action in matrix form

$$\overbrace{\begin{pmatrix} \omega_\alpha \\ \omega_\beta \\ \omega_\gamma \end{pmatrix}}^{\omega} = \overbrace{\begin{pmatrix} 1 & 0 & -\sin(\beta) \\ 0 & \cos(\alpha) & \cos(\beta)\sin(\alpha) \\ 0 & -\sin(\alpha) & \cos(\alpha)\cos(\beta) \end{pmatrix}}^{T_g L_{g^{-1}}} \overbrace{\begin{pmatrix} \dot{\alpha} \\ \dot{\beta} \\ \dot{\gamma} \end{pmatrix}}^{\dot{g}}. \tag{13}$$

The above equation allows us to verify the Lagrangian invariance by computing and comparing the quantities, $L((g, r), (\dot{g}, \dot{r}))$ and $L((L_{g^{-1}} g, r), (T_g L_{g^{-1}} \dot{g}, \dot{r}))$. After verifying the invariance of the Lagrangian we can compute the reduced Lagrangian and the reduced mass matrix. The components of the reduced mass matrix, as given in (6), are computed for the pivoting dynamic model where

Downloaded from ijr.sagepub.com at PENNSYLVANIA STATE UNIV on May 16, 2016

Table 2. The local form of the locked inertia tensor for the reduced mass matrix.

$$I(r) = \begin{pmatrix} H^2 + 2R^2 & HR(-\cos(\sigma_1) + \cos(\sigma_2)) & HR(-\sin(\sigma_1) + \sin(\sigma_2)) \\ HR(-\cos(\sigma_1) + \cos(\sigma_2)) & (5H^2 + R^2) - \frac{R^2}{2}(\cos(2\sigma_1) + \cos(2\sigma_2)) & -\frac{R^2}{2}(\sin(2\sigma_1) + \sin(2\sigma_2)) \\ HR(-\sin(\sigma_1) + \sin(\sigma_2)) & -\frac{R^2}{2}(\sin(2\sigma_1) + \sin(2\sigma_2)) & (4H^2 + R^2) + \frac{R^2}{2}(\cos(2\sigma_1) + \cos(2\sigma_2)) \end{pmatrix}$$

$$I(r)A(r) = \begin{pmatrix} 2R^2 & 2R^2 \\ -2HR\cos(\sigma_1) & 2HR\cos(\sigma_2) \\ -2HR\sin(\sigma_1) & 2HR\sin(\sigma_2) \end{pmatrix}, \quad (14)$$

$$m(r) = \begin{pmatrix} 2R^2 & 0 \\ 0 & 2R^2 \end{pmatrix}, \quad (15)$$

where $I(r)$ is given in Table 2. Note that as expected the reduced mass matrix depends solely on the base variables σ_1 and σ_2.

Example 2: Kinematic Snake Robot

The second example system is the kinematic snake robot which is composed of three rigid links that are connected by two revolute joints and three passive wheel sets connected to each link (Figure 2). This robot is similar to the kinematic snake studied by Ostrowski (1995). For our system, the wheel axes are rigidly held perpendicular to the links while Ostrowski actually controlled the angles between the wheel axes and the links, hence increasing the dimension of the base space. Even though we fix the angles of the wheel axes with respect to the links, we are still able to generate gaits to move the kinematic snake in the plane.

We attach a body coordinate frame to the middle of the center link as shown in Figure 2. The position and orientation of this body frame is represented by the three fiber variables, (x, y, θ), which denote position of the origin of the body frame and its orientation in the plane. The two internal degrees of freedom are represented by the relative angle between the links (α_1, α_2).

Similarly, the kinematic snake has a five-dimensional, $(n = 5)$, configuration space $Q = G \times M$, where the associated Lie group fiber space denoting the robot's orientation in the plane is $G = \mathrm{SE}(2)$, the special Euclidean group. The base space denoting the internal degrees of freedom is $M = \mathbb{S} \times \mathbb{S}$. Note that we do not care about the mass and inertia of this system because, as we show later, it is principally kinematic and all of the momentum variable are annihilated. In other words, if we lock the base variables of the kinematic snake, away from singular base configurations, the kinematic snake cannot move in any direction because the non-holonomic constraints fully span the fiber space. Thus, there are no allowable directions of motion along which we can define any momentum variables.

There are three non-holonomic constraints acting on the kinematic snake. Each of them has the following form

$$\begin{pmatrix} \dot{x}_i & \dot{y}_i \end{pmatrix} \begin{pmatrix} \cos(\theta_i) \\ \sin(\theta_i) \end{pmatrix} = 0,$$

where (x_i, y_i) is the global[1] position of the intersection point of the wheel axes and the snake links, and θ_i is the global orientation of the wheel axes.

Given that the fiber space has an SE(2) group structure, we can compute the group action and lifted action. In particular, the matrix form of the lifted action is given by

$$\overbrace{\begin{pmatrix} \xi_1 \\ \xi_2 \\ \xi_3 \end{pmatrix}}^{\xi} = \overbrace{\begin{pmatrix} \cos(\theta) & -\sin(\theta) & 0 \\ \sin(\theta) & \cos(\theta) & 0 \\ 0 & 0 & 1 \end{pmatrix}}^{T_g L_{g^{-1}}} \overbrace{\begin{pmatrix} \dot{x} \\ \dot{y} \\ \dot{\theta} \end{pmatrix}}^{\dot{g}}. \quad (16)$$

Using the above equation we can compute the non-holonomic constraints, $\omega(q)\dot{q} = 0$, in body coordinates. This is simply done by inverting (16) to obtain $\dot{g} = (T_g L_{g^{-1}})^{-1}\xi$ and substituting the fiber velocity, $\dot{g}$, by its body representation, ξ, in (3). Then we verify that the constraints are independent of any fiber variables as shown in the following equation

$$\begin{pmatrix} -\sin(\sigma_1) & \cos(\sigma_1) & -R - H\cos(\sigma_1) \\ 0 & 1 & 0 \\ \sin(\sigma_2) & \cos(\sigma_2) & R + H\cos(\sigma_2) \end{pmatrix} \begin{pmatrix} \xi_1 \\ \xi_2 \\ \xi_3 \end{pmatrix} + \begin{pmatrix} -R & 0 \\ 0 & 0 \\ 0 & -R \end{pmatrix} \begin{pmatrix} \dot{\sigma}_1 \\ \dot{\sigma}_2 \end{pmatrix} = 0. \quad (17)$$

1. Global means that the position is represented in a fixed inertial frame.

Downloaded from ijr.sagepub.com at PENNSYLVANIA STATE UNIV on May 16, 2016

5. Mechanical Systems Classification

In this section we build upon the background material presented in Section 10 and tailor the results into new forms that serve our gait generation techniques. Even though some of the results seen in this section could be found in prior work, we alternatively attain the same results in what we believe to be a rather more compact and direct method. First, we classify mechanical systems into three major classes, where the second class has two subclasses.

5.1. Purely Mechanical Systems

Purely mechanical systems are systems whose Lagrangian is comprised solely of the kinetic energy such that the Lagrangian is also invariant with respect to the group actions. This allows us to solve for the reduced Lagrangian which is itself independent of the group variables. Moreover, the system is not subjected to any external forces, that is, $\tau^e = 0$ from (10). Finally, the system starts from rest, that is, its initial momentum is zero. For such systems, the reconstruction and momentum evolution equations reduce to

$$\xi = -A(r)\dot{r}, \tag{18}$$

$$\dot{p} = p = 0, \tag{19}$$

where $A(r)$ is the local form of the mechanical connection as defined above.

5.2. Kinematic Systems

According to Choset et al. (2005), a mechanical system is *kinematic* when the first derivative of its state vector is linearly dependent on the control inputs, that is, $\dot{q} = A(q)u$ where q is a state vector, $A(q)$ is a matrix and u is the input vector. We distinguish between two types of kinematic systems:

1. *Purely kinematic systems*. These are defined as systems that have as many independent non-holonomic constraints as the dimension of the system's fiber space. The motion of such systems with a configuration $q = (g, r) \in Q$ can be described by the reconstruction equation, $\xi = A(g, r) \cdot \dot{r}$, where ξ is the body representation of an l-dimensional fiber velocity, $A(g, r)$ is an $l \times m$ matrix that depends on the configuration q and we treat $\dot{r}$ as an m-dimensional input vector.

2. *Principally kinematic systems*. Moreover, if the non-holonomic constraints of the purely kinematic system are *invariant* with respect to group action, the mechanical system becomes principally kinematic. We show later how the motion of principally kinematic systems is governed solely by base motions and the prescribed non-holonomic constraints.

In this paper, we are interested in the second type of kinematic systems and we give its technical definition as follows.

Definition 1. [Principally kinematic system] Given a mechanical system that has an n-dimensional configuration space with trivial principal fiber structure, $Q = G \times M$, where l and m denote the dimensions of G and M, respectively, with $n = l + m$, and the mechanical system is subjected to k non-holonomic constraints, $\omega(q) \cdot \dot{q} = 0$, where the dimension of the matrix ω is $k \times n$, such a system is said to be principally kinematic[2] if:

- $0 < k < l$ (the number of constraints is less than dimension of fiber space);
- $\text{rank}(\omega(q)) = k$ (the constraints are linearly independent);
- $\omega(q) \cdot \dot{q} = \omega(\Phi_g(q)) \cdot T_g\Phi_g(\dot{q}) = 0$ (the constraints are invariant with respect to the Lie group actions);

where $\Phi_h q = (L_h g, r)$ and $T_q\Phi_h\dot{q} = (T_g L_h \dot{g}, \dot{r})$ are the action and lifted action induced by the Lie group structure of the fiber space.

In the case of principally kinematic systems, the reconstruction and momentum evolution equations reduce to

$$\xi = -\mathbb{A}(r)\dot{r}, \tag{20}$$

$$p \text{ is not defined.} \tag{21}$$

where $\mathbb{A}(r)$ is the local form of the kinematic connection. Note that in this case there are no momentum variables because they are totally annihilated by the constraints as shown in (21).

5.3. Mixed Non-holonomic Systems

Finally, for the sake of completeness, we very briefly mention a third class of mechanical systems, mixed non-holonomic systems. Mixed systems are interesting because they have non-holonomic constraints which exclude them from being purely mechanical; in addition, such systems do not have enough non-holonomic constraints to be classified as principally kinematic. One can think of mixed system as a generalization of both purely mechanical and principally kinematic systems. In fact, we study this third type of system in the companion paper (Shammas et al. 2007).

Before we demonstrate how to compute the connections for these types of mechanical systems, we verify to what classes our two example systems belong.

Example 1: Pivoting Dynamic Model

We have already verified the invariance of the Lagrangian and there are no external forces acting on the pivoting dynamic model. Thus, if the system starts at rest, then all angular momentum variables will remain constant and equal to zero for all time. We conclude that the pivoting dynamic model is a *purely mechanical* system.

2. Sometimes, these systems are referred to as *Chaplygin*.

Downloaded from ijr.sagepub.com at PENNSYLVANIA STATE UNIV on May 16, 2016

Example 2: Kinematic Snake Robot

We have already verified that the set of non-holonomic constraints are invariant with respect to the Lie group action. Moreover, we know that away from singular configurations, the non-holonomic constraints are linearly independent. Finally, we have three non-holonomic constraints, which is equal to the dimension of the fiber space, SE(2). Hence, the kinematic snake robot is a *principally kinematic* system.

6. Computing the Reconstruction Equations

In this section we compute the connections for both the purely mechanical and principally kinematic systems. We verify that both systems have *structurally* similar reconstruction equations. Recall that for a mechanical system whose Lagrangian and non-holonomic constraints are invariant with respect to its fiber space group action and lifted action, the reduced Lagrangian (5) and reduced non-holonomic constraints (8) can respectively be rewritten as

$$l(\xi, r, \dot{r}) = \frac{1}{2}\begin{pmatrix}\xi & \dot{r}\end{pmatrix}^{\mathrm{T}}\begin{pmatrix} I & IA \\ (IA)^{\mathrm{T}} & m\end{pmatrix}\begin{pmatrix}\xi \\ \dot{r}\end{pmatrix}, \quad (22)$$

$$\bar{\omega}_\xi \xi = -\bar{\omega}_r \dot{r}, \quad (23)$$

where I is the local form of the locked inertia tensor, A is the local form of the mechanical connection, $\bar{\omega}_\xi$ and $\bar{\omega}_r$ are submatrices of the constraint matrix $\bar{\omega}$ as shown in Lemma B.1 in Appendix B. All of the above matrices are independent of the fiber variable, g, and depend only on the shape variables, r. Define the *generalized non-holonomic momentum* along the allowable fiber directions by

$$p = \frac{\partial l}{\partial \xi}\bar{\Omega}^{\mathrm{T}}$$

where $\bar{\Omega}^{\mathrm{T}}$ is a basis of $\mathcal{N}(\bar{\omega})$, the null space of $\bar{\omega}$. Then using (22) we have

$$p = \frac{\partial l}{\partial \xi}\bar{\Omega}^{\mathrm{T}} = (\xi^{\mathrm{T}} I^{\mathrm{T}} + \dot{r}^{\mathrm{T}}(IA)^{\mathrm{T}})\bar{\Omega}^{\mathrm{T}}. \quad (24)$$

Rewriting (23) and (24) we obtain

$$\bar{\omega}_\xi \xi = -\bar{\omega}_r \dot{r}, \quad (25)$$

$$\bar{\Omega} I \xi = p^{\mathrm{T}} - \bar{\Omega} I A \dot{r}. \quad (26)$$

Using the above two equations, we can solve for the connection for both the purely mechanical and principally kinematic systems:

- *Purely mechanical systems*. These are systems that are not subject to any velocity constraints, that is, $\bar{\omega}_\xi = \mathbf{0}^{l\times l}$ and $\bar{\Omega} = \mathbf{I}^{l\times l}$, where $\mathbf{0}^{l\times l}$ and $\mathbf{I}^{l\times l}$ are $l \times l$ zero and identity matrices, respectively. Moreover, because momentum is zero for all times, $p = \mathbf{0}^{1\times l}$. Then (26) becomes
$$\xi = -A(r)\dot{r}, \quad (27)$$
where $A(r)$ is the local form of the mechanical connection seen in (18).
- *Principally kinematic systems*. These are systems that have l linearly independent velocity constraints, that is, $k = l$. In this case, $\bar{\omega}_\xi$ is full rank and $\bar{\Omega} = \mathbf{0}$. Then (26) is trivially satisfied and we can solve for ξ from (25)
$$\xi = -\bar{\omega}_\xi^{-1}\bar{\omega}_r \dot{r} = -\mathbb{A}(r)\dot{r}, \quad (28)$$
where $\mathbb{A}(r)$ is the local form of the principally kinematic connection seen in (20).

Thus, we have verified that the mechanical connection and the principally kinematic connection can be easily obtained from the reduced mass matrix of a purely mechanical system and the reduced non-holonomic constraints of a principally kinematic system, respectively. We now revisit the example systems and compute their respective connections.

Example 1: Pivoting Dynamic Model

Using (6), the local from of the mechanical connection, $A(r)$, can be computed directly by inverting $I(r)$ from Table 2 and post-multiplying it by $I(r)A(r)$ from (14). Then $A(r)$ will have the following form

$$A(r) = \begin{pmatrix} f_1^1(\sigma_1, \sigma_2) & f_2^1(\sigma_1, \sigma_2) \\ f_1^2(\sigma_1, \sigma_2) & f_2^2(\sigma_1, \sigma_2) \\ f_1^3(\sigma_1, \sigma_2) & f_2^3(\sigma_1, \sigma_2)\end{pmatrix},$$

where f_j^i are the ith row and jth column of the mechanical connection which are analytic functions of the base variables (σ_1, σ_2). We do not present the expression of the f_j^i functions in the paper; however, these expressions can be computed in the Mathematica® code included in Extension 1.

Example 2: Kinematic Snake Robot

Similarly, for the kinematic snake robot we can compute the local form of the kinematic connection, which will have the following form:

$$\mathbb{A}(r) = \frac{R}{D}\begin{pmatrix} R + H\cos(\sigma_2) & R + H\cos(\sigma_1) \\ 0 & 0 \\ -\sin(\sigma_2) & -\sin(\sigma_1)\end{pmatrix}$$

Downloaded from ijr.sagepub.com at PENNSYLVANIA STATE UNIV on May 16, 2016

where $D = R\sin(\sigma_1) + L\sin(\sigma_1 - \sigma_2) - R\sin(\sigma_2)$ and again the components of the connection's local form are analytic functions of the base variables (σ_1, σ_2).

Having computed the connections, we present our gait generation analysis next and then generate gaits for the above two examples.

7. Gait Evaluation and Synthesis

We define a *gait* as a closed curve, γ, in the base space, M, of the robot. We require that our gaits be cyclic, that is, the system will retain its original shape after each period of time; moreover, we require γ to be continuous. Previously we have proved that the reconstruction equations for both the purely mechanical and principally kinematic systems are identical in structure. Both have the following form

$$\xi = -\mathbf{A}(r)\dot{r}, \tag{29}$$

where $\mathbf{A}(r)$ can denote either the purely mechanical connection $A(r)$ or the principally kinematic connection $\mathbb{A}(r)$. Next, we integrate (29) with respect to time. For each row, the left-hand side yields a position change in body coordinates while the integrand of the right-hand side becomes a one-form.

7.1. Gait Evaluation

First define the variable ζ as the integral of ξ, that is, $\dot{\zeta} = \xi$, then integrating a row of (29) with respect to time we obtain

$$\begin{aligned}\Delta\zeta^i &= \int_{t_0}^{t_1} \dot{\zeta}^i\, dt = \int_{t_0}^{t_1} \xi^i\, dt \\ &= -\int_{t_0}^{t_1} \sum_j \mathbf{A}^i_j(r)\dot{r}^j\, dt \\ &= -\oint_{\gamma(r)} \sum_j \mathbf{A}^i_j(r)\, dr^j. \end{aligned} \tag{30}$$

Thus, we relate a position change along a fiber direction, $\Delta\zeta^i$, to a line integral along the base space curve, $\gamma(t)$. This will help us to formalize the gait synthesis problem.

7.2. Gaits Synthesis

In this section we formulate a variational problem that maximizes the fiber motion magnitude for all gaits with a given length.

Even though the variational problem for generating optimal gaits is well defined in higher dimensions, we formalize the problem in two dimensions for the sake of clarity and simplicity. Each row of $\mathbf{A}(r)\,dr$ is a two-dimensional one-form, that is, $(\mathbf{A}(r)\,dr)^i = f_1^i(r^1, r^2)\,dr^1 + f_2^i(r^1, r^2)\,dr^2$ where $r = (r^1, r^2)$ is comprised of the base variables. Then, the functional which we are optimizing is a one-form

$$J^i(\gamma) = \oint_\gamma f_1^i(r^1, r^2)\,dr^1 + f_2^i(r^1, r^2)\,dr^2. \tag{31}$$

For this problem it is convenient to parameterize the gait by its arc length, s. This will yield a well-defined functional to be maximized

$$\begin{aligned}&\max J^i(\gamma(s)) \\ &= \max \int_{s_0}^{s_1} \left(f_1^i(r^1, r^2)\frac{\partial r^1}{\partial s} + f_2^i(r^1, r^2)\frac{\partial r^2}{\partial s} \right) ds. \end{aligned} \tag{32}$$

Next we enforce an essential fixed gait length requirement. This constraint on the length of the curves is represented by the following integral

$$L = \int_{s_0}^{s_1} \sqrt{\left(\left(\frac{\partial r^1}{\partial s}\right)^2 + \left(\frac{\partial r^2}{\partial s}\right)^2 \right)}\, ds. \tag{33}$$

If such a bound is not enforced we can obtain an unbounded integral, J, for a gait with unbounded length. The above two integrals in (32) and (33) define a constrained calculus of variations problem. Nonetheless, the integrands of the above equations are usually complicated functions, hence the differential equations that the Euler–Lagrange solution equations yield are very complicated to solve. Thus, to solve the variational problem, we are forced to use numerical techniques.

It is worth noting that we do not utilize the synthesis we presented in the section to generate gaits. The formulation of the variational problem presented in this section is similar to that presented by Ostrowski et al. (2000) for designing *optimal* gaits; however, Ostrowski et al. limited themselves to sinusoidal gaits and they numerically solved for optimal gaits by minimizing an energy functional $\int_0^1 \dot{r}^{\mathrm{T}}\dot{r}\, dt$ with appropriate boundary conditions that specify the change in position.

8. Analysis of Geometric Gaits

One could design gaits by proposing (that is, guessing) a gait and then numerically evaluating the motion due to each proposed gait. Not only is this approach tedious, it is also incomplete. In addition, one can limit the search space of gaits to a certain type, such as sinusoidal gaits, as was the case in most of the prior work; however, such a restriction might exclude other families of gaits which might be optimal with respect to some metrics.

At this point we set ourselves apart from the prior work and rather than numerically solving the above constrained variational problem or limiting ourselves to a certain type of gaits,

Downloaded from ijr.sagepub.com at PENNSYLVANIA STATE UNIV on May 16, 2016

we use Stokes' theorem to transform the line integral in (30) to a volume integral. This will provide us with a simple gait evaluation technique that measures the motion contribution resulting from *any* closed curve in the base space. Actually, this evaluation tool is simple enough that we can utilize it to actually synthesize gaits.

Note that the integrand in (30), $\sum_j \mathbf{A}^i_j(r)dr^j$, is a one-form, hence we can use Stokes' theorem to transform the integral to an integral of a two-form which is the exterior derivative of the original one-form. Thus, we rewrite the change in position expressed in body coordinates as

$$\begin{aligned}\Delta\zeta^i &= \iint_\Gamma \sum_{o,j=1,o<j}^{m} (\bar{\mathbf{A}}^i_{oj}(r))\, dr^o\, dr^j \\ &= \sum_{o,j=1,o<j}^{m} \iint_\Gamma F^i_{oj}(r)\, dr^o\, dr^j, \end{aligned} \tag{34}$$

where Γ is the region enclosed by the gait γ. Note that, $\Delta\zeta^i$ is equated to the double integral of the integrands, $F^i_{oj}(r)$, which are the components of the two-form. Hence, we have equated the position change for any closed curve in the base space, γ, to the volume that this curve envelops under several well-defined functions. Note that these height functions are simply composed of partial derivatives of the components of the connection matrix with respect to the base variables. By studying the properties of these height functions we are actually able to design curves that produce a desired $\Delta\zeta^i$.

Thus, we synthesize gaits by only analyzing the components of the two-form $\bar{\mathbf{A}}^i_{oj}(r)$. We refer to these gaits as *geometric* since the resulting motion is strictly due to the geometric phase shift of the designed gait. For simplicity, let us assume that we have two base variables, then by using Green's theorem, the two-dimensional version of Stokes' theorem, the position change given in (34) becomes

$$\Delta\zeta^i = \iint_\gamma \overbrace{\left(\frac{\partial f^i_2(r)}{\partial r^1} - \frac{\partial f^i_1(r)}{\partial r^2}\right)}^{F^i(r)} dr^1\, dr^2. \tag{35}$$

By studying the integrands in (35) and by designing and placing curves in the base space, we are able to generate gaits that move the mechanical system along a desired direction.

We remind the reader that $\Delta\zeta^i$ is an integral of a body representation of a fiber velocity ξ^i. Hence, it does not necessarily relate trivially to inertial position change, Δg^i. This is the case only when the fiber has a commutative group structure, that is, the lifted action map is the identity map.

8.1. Properties of Height Functions

By studying the structure of the integrand functions of (35) we are able to evaluate the motion of the system due to closed curves in the base space. We refer to the integrand functions as *height functions*[3] in the rest of the paper. We study the following properties of the height functions.

8.1.1. Symmetry

We study periodicity which allows us to investigate smaller portions of the base space. Moreover, we find the set of points or lines about which the height function is even or odd. For example, a gait that is symmetric about an odd point of the height function yields zero fiber motion.

8.1.2. Signed Regions

Since we are integrating a height function over a closed region, it is important to know where the height function is positive, negative or zero. Not only does this allow us to control the direction of motion along the fiber variables but also to optimize gaits by restricting them to lie in a strictly positive or negative region.

8.1.3. Unboundedness

While designing gaits, one should stay away from regions where the height functions tend to infinity. A gait that passes through such regions may yield infinite volume, that is, infinite position change for finite shape changes. Usually this is an indication that a non-holonomic constraint is being violated or that the system has passed through a problematic singularity.

By inspecting the above properties of the height functions we are able to evaluate the position change of the robot due to following any closed curve in the base space.

8.2. Gait Generation with Height Functions

Thus far, we have related motion along the fiber to an oriented volume integral in the base space. Hence, we can compute how the robot's position changes as it changes its shape along *any* closed curve in the base space. Since our gait evaluation technique is direct and simple we can devise a set of simple rules that can be used to generate gaits.

8.2.1. Non-self-intersecting Curves

Any closed non-self-intersecting curve that lies entirely in a positive or negative region is guaranteed to produce a non-zero fiber motion.

3. Note that we have l height functions where l is the dimension of the fiber space G.

Downloaded from ijr.sagepub.com at PENNSYLVANIA STATE UNIV on May 16, 2016

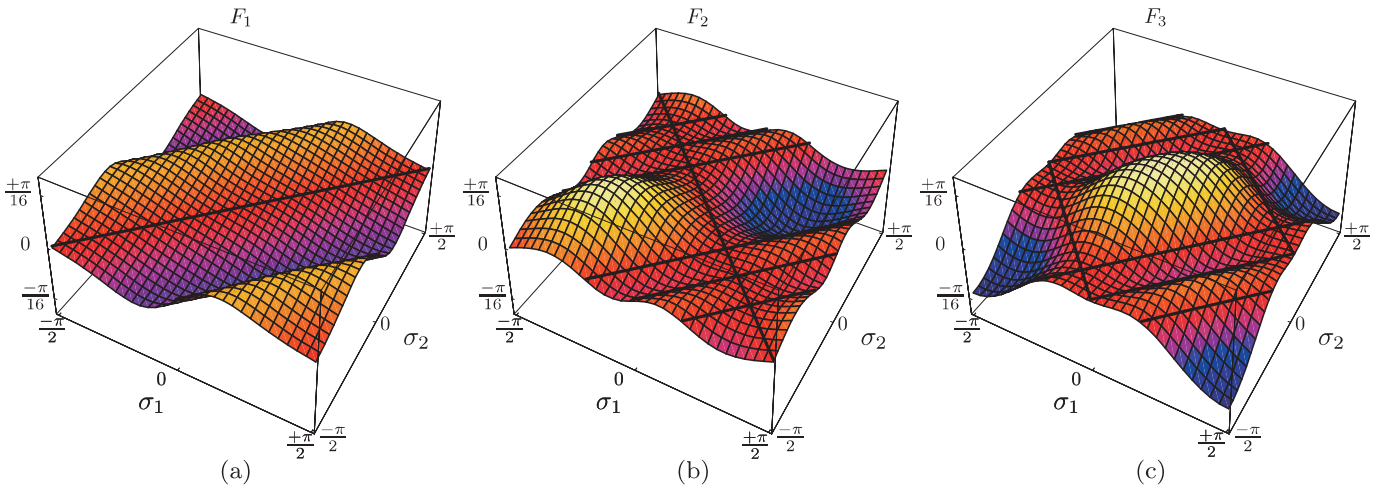

Fig. 3. The height functions corresponding to the three fiber directions expressed in body representation, $(\omega_\alpha, \omega_\beta, \omega_\gamma)$, for the pivoting dynamic model. Darker colors of the height functions denote the negative regions while lighter colors denote the positive regions. The solid curves indicate the zero lines that separate the positive from the negative regions. Note that these curve are not all straight lines.

8.2.2. Self-intersecting Curves

Any closed self-intersecting curve is guaranteed to produce a non-zero fiber motion provided that the curve spans two regions of opposite signs, the self-intersection occurs along the zero line separating the two regions and the curve changes orientation as it passes from one region to the other.

8.2.3. Symmetric Non-intersecting Curves Around "Odd" Points

Let K_{odd} be the set of all points about which the height function is odd. Then any curve symmetric with respect to points in K_{odd} will enclose equal areas in two or more adjacent regions that have opposite signs. Integrating the volume under such curves will yield zero, that is, the fiber motion for such gaits is identically zero.

8.2.4. Symmetric Intersecting Curves Around "Even" Points

Let K_{even} be the set of all points about which the height function is even along a fixed direction. For any self-intersecting curve symmetric with respect to points in K_{even} along the specified direction, the intersection will occur in the set K_{even}. For curves that change orientation at the intersection point, they will enclose equal areas but of opposite orientation signs; hence, such curves will yield zero volume, that is, the fiber motion for such gaits is identically zero.

These rules do not impose any additional constraints on the shape of the input curves. For instance, as long as the curve stays entirely in one region and does not intersect itself, it is guaranteed to generate a non-zero fiber motion. The larger the area enclosed by the curve within a positive or negative region, the larger the generated geometric phase shift.

Moreover, this approach eliminates the restriction of sinusoidal inputs that was required in prior work. Finally, the first two rules are "active" rules which help in designing gaits that produce motion, while the last two rules are "passive" rules that ensure null motion of the system. All rules are equally as important as we use the first two rules to produce motion along a specified height function while the last two rules are used to ensure zero motion along the rest of the fiber variables.

Example 1: Pivoting Dynamics Model

We now revisit the pivoting dynamic model and generate gaits for it using our gait analysis as presented above. In particular, we set the robots' point masses to $m = 1$, and the parameters $H = 1$ and $R = 1$. Then we can compute the height functions by utilizing Green's theorem. The three height functions corresponding to the three fiber directions are shown in Figure 3.

All three height functions have distinctive signed regions. The darker colors denote the negative regions while the lighter colors denote the positive regions. Note that none of the height functions has unbounded regions. In fact, this is a property of all purely mechanical systems. The intuition behind why the height functions for purely mechanical systems are always bounded is that for whatever base motion the robot is forced to do, the system always has bounded motion, that is, a bounded volume under the height functions. In other words, there are no singularities of motion.

Downloaded from ijr.sagepub.com at PENNSYLVANIA STATE UNIV on May 16, 2016

Without loss of generality, we assume that we want to design a gait that rotates the robot *only* around the x-axis. This means that we want to design a gait that envelops a non-zero volume only under the *first* height function in Figure 3. To design such a curve, we should look carefully at the height functions' properties. Note that the first height function in Figure 3 is odd about the line $\sigma_2 = \sigma_1$ and even about the line $\sigma_2 = -\sigma_1$. The second height function is even about the line $\sigma_2 = \sigma_1$ and odd about the line $\sigma_2 = -\sigma_1$. Finally, the third height function is even about both lines. Thus, we can see that a figure-eight type of curve with the following properties will envelop volume only under the first height function:

(i) The curve is centered at the origin of the base space.

(ii) Each of the curve loops are on either side of the line $\sigma_2 = \sigma_1$.

(iii) The curve is symmetric with respect to the two lines $\sigma_2 = \sigma_1$ and $\sigma_2 = -\sigma_1$.

(iv) The curve is bounded by the two lines $\sigma_2 = \sigma_1 - \pi$ and $\sigma_2 = \sigma_1 + \pi$.

The curve G_1^{PDM} in (36) satisfies all of the above conditions:

$$G_1^{\text{PDM}}: \quad \begin{aligned} \sigma_1 &= \frac{\pi}{2}(\sin(t) + \sin(2t)), \\ \sigma_2 &= \frac{\pi}{2}(-\sin(t) + \sin(2t)). \end{aligned} \tag{36}$$

We have used second rule for the first height function and the fourth rule for the second and third height function. Note that we bounded the curve between the two lines $\sigma_2 = \sigma_1 - \pi$ and $\sigma_2 = \sigma_1 + \pi$ so that each loop of the figure-eight curve stays within the same-signed region.

The G_1^{PDM} gait is shown in the first column of Figure 4. We have numerically simulated this gait and indeed as expected the robot rotated only around the x-axis after one complete cycle. The rotations along all three axes are shown in the last row of the first column of Figure 4. Note that there are no net rotations about other two axes, y and z, at the end of the gait cycle.

Similarly, we can design two other gaits, G_2^{PDM} and G_3^{PDM}, given in (37) and (38), respectively, that will independently rotate the robot only around either the y- and z-axis:

$$G_2^{\text{PDM}}: \quad \begin{aligned} \sigma_1 &= \frac{\pi}{4}(2\sin(t) + \sin(2t)), \\ \sigma_2 &= \frac{\pi}{4}(2\sin(t) - \sin(2t)), \end{aligned} \tag{37}$$

$$G_3^{\text{PDM}}: \quad \begin{aligned} \sigma_1 &= \frac{\pi}{4}(2\sin(t) + \cos(t)), \\ \sigma_2 &= \frac{\pi}{4}(2\sin(t) - \cos(t)). \end{aligned} \tag{38}$$

We have constructed such gaits and they are shown in the second and third columns of Figure 4. We have plotted the initial and final configuration of the pivoting dynamic model for each the three gaits as shown in Figure 5 where the three independent rotations, $\Delta\alpha$, $\Delta\beta$ and $\Delta\gamma$, are depicted. To understand the motion of the pivoting dynamic model throughout a gait, we divided the entire motion of the system while performing the gait G_1^{PDM} into smaller intervals and depicted both the body motion and total motion as shown in Figure 6.

Hence, using our gait generation analysis we were able to easily design three gaits each of which moves the robot independently along one fiber direction.

Example 2: Kinematic Snake Robot

As for the kinematic snake robot, its height functions are given by

$$\begin{aligned} F_1^{\text{KS}} &= \Big[2HR + (H^2 + R^2)\cos(\sigma_2) \\ &+ \cos(\sigma_1)(H^2 + R^2 + 2HR\cos(\sigma_2))\Big] \\ &\times \Big[-\frac{4}{R}\Big(H\cos\Big(\frac{\sigma_1 - \sigma_2}{2}\Big) \\ &+ R\cos\Big(\frac{\sigma_1 + \sigma_2}{2}\Big)\Big)^2 \sin\Big(\frac{\sigma_1 - \sigma_2}{2}\Big)^2\Big]^{-1} \\ F_2^{\text{KS}} &= 0 \\ F_3^{\text{KS}} &= \Big[R\sin\Big(\frac{\sigma_1 + \sigma_2}{2}\Big)\Big] \\ &\times \Big[2\Big(H\cos\Big(\frac{\sigma_1 - \sigma_2}{2}\Big) \\ &+ R\cos\Big(\frac{\sigma_1 + \sigma_2}{2}\Big)\Big)\sin\Big(\frac{\sigma_1 - \sigma_2}{2}\Big)^2\Big]^{-1}. \end{aligned}$$

In particular, we choose the robot parameters to be $H = 1$ and $R = 1$. A plot of the three height functions for such a kinematic snake are shown in Figure 7. The first two height functions correspond to ξ^1 and ξ^2 fiber translations while the third height function corresponds to ξ^3 fiber rotation. Note that the second height function is always zero. This is because we aligned the second axis of the body frame along the wheel axis of the middle link as shown in Figure 2. This means that for an observer sitting on the robot, there will never be any motion along the wheel axis due to the no-sideways-motion nonholonomic constraint.

Moreover, note that the first and third height functions have unbounded regions. To be able to plot these unbounded

Downloaded from ijr.sagepub.com at PENNSYLVANIA STATE UNIV on May 16, 2016

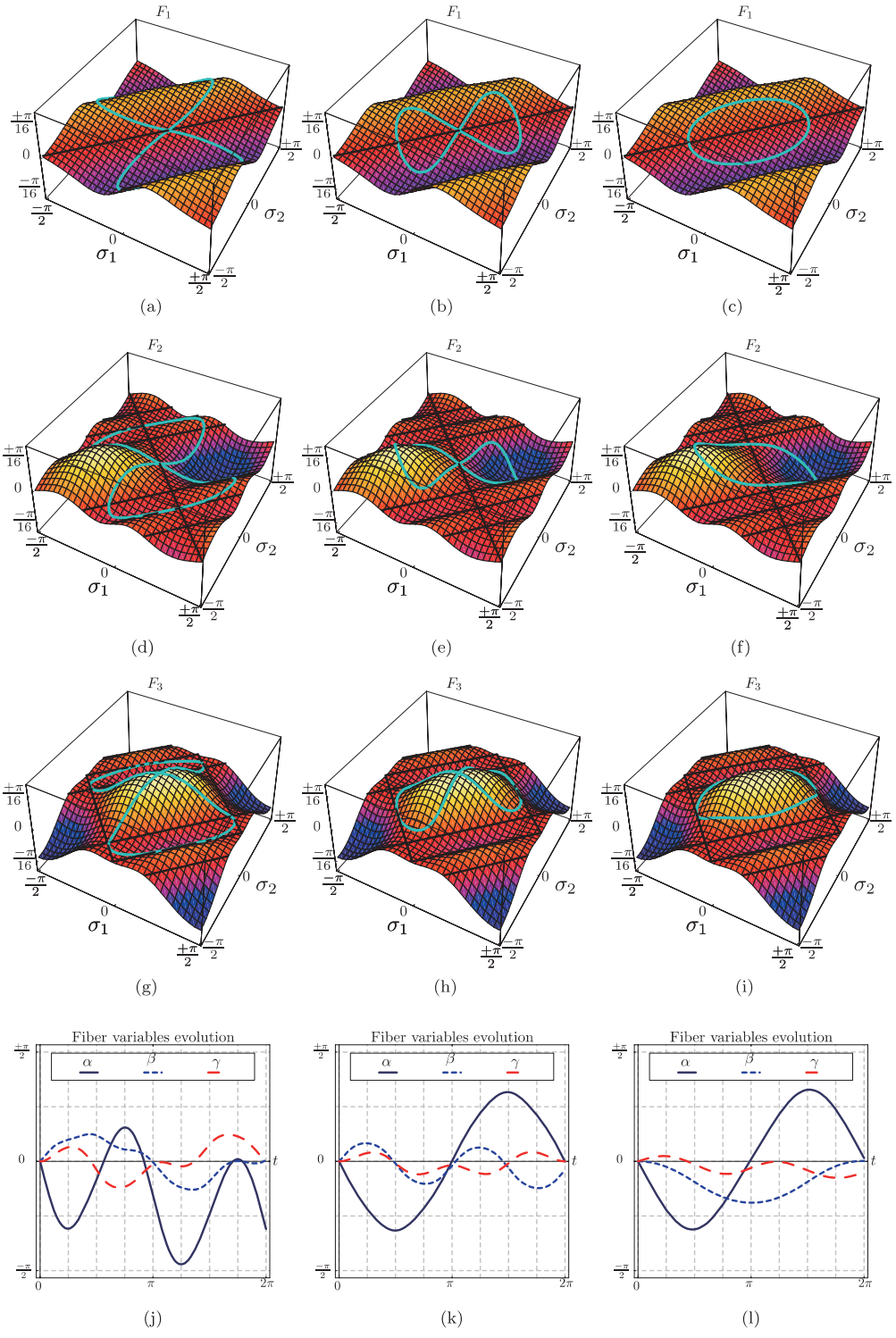

Fig. 4. Three sample gaits, (G_1^{PDM}, G_2^{PDM}, G_3^{PDM}), that were designed to rotate the pivoting dynamic model independently along each of the three rotation axes. The first column depicts a gait that rotates the robot around the x-axis, while the second and third rows depict gaits that rotate the robot around the y- and z-axes, respectively. Note that the solid dots on the gait curves in the first three rows indicate the initial shape of the pivoting dynamic model for each of the gaits. The last row of each column depicts a time simulation of each gait where the rotations around each axis are plotted versus time.

Downloaded from ijr.sagepub.com at PENNSYLVANIA STATE UNIV on May 16, 2016

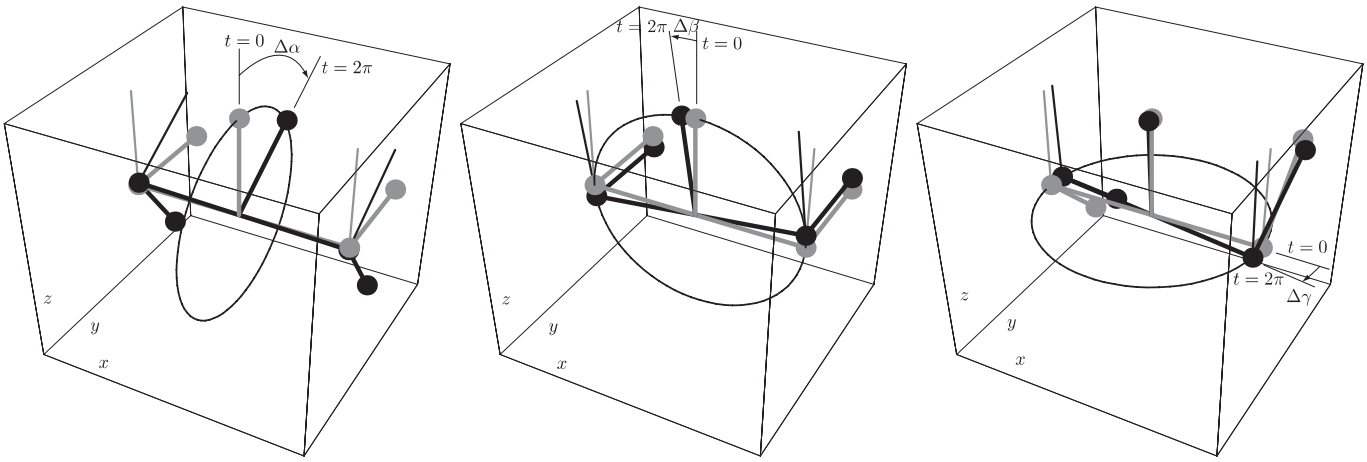

Fig. 5. Snapshots of the pivoting dynamic model at the beginning and the end of each period of the simulated gaits, G_1^{PDM}, G_2^{PDM} and G_3^{PDM}. Note the independent rotations, $\Delta\alpha$, $\Delta\beta$ and $\Delta\gamma$ around the x-, y- and z-axes, respectively. In the first plot, the robot retains its original shape (shown in gray), but it has rotated as a whole around the x-axis to its final position (shown in black). The motion of the middle mass is depicted by the circle. The same is true for the second two plots where the robot rotates as a whole around the y- and z-axes, respectively, as depicted by the circles.

height regions, we used the arc-tangent function to map the range of the height functions to the interval $[-\pi/2, \pi/2]$. These regions are depicted by the dashed lines shown in Figure 7. These unbounded regions correspond to a singular configuration of the robot, where one or more of the non-holonomic constraints becomes a linear combination of the others. For example, consider the line $\sigma_2 = -\sigma_1$ in Figure 7. At this line both the first and third height functions have infinite values which we plot at $\pm\pi/2$. This line corresponds to snake configurations where all three wheel axes meet at a single point. It is intuitively clear that if the robot starts at such a configuration it cannot change its conf iguration without breaking one of the non-holonomic constraints, that is without one of the wheels sliding sideways.

On the other hand, consider a gait that contains a portion of the line $\sigma_2 = -\sigma_1$. The volume under the height function for such a gait will be unbounded, that is, for a finite base variable change, the snake will have infinite motion. Such a gait is not feasible. Hence, not only do these height functions help us in designing gaits, they also depict singularity regions in the base space.

Again, without loss of generality, assume that we want to design a gait that will rotate the kinematic snake, that is, move the system along the θ fiber direction. In other words, we want to design a curve that will envelop non-zero volume only under the third height function. Note that the first height function for the kinematic snake is even about both lines $\sigma_2 = \sigma_1$ and $\sigma_2 = -\sigma_1$, while the third height function is even about the line $\sigma_2 = -\sigma_1$ and odd about the line $\sigma_2 = \sigma_1$. So to move the robot in the θ direction we need a figure-eight type of curve with the following properties:

- The curve is centered at the line $\sigma_2 = \sigma_1$.
- Both of the curve loops are on either side of the line $\sigma_2 = \sigma_1$.
- The curve is symmetric with respect to a line parallel $\sigma_2 = -\sigma_1$.

The curve G_3^{KS} in (41) satisfies all of the above conditions. Again, we used the second rule on the third height function and the fourth rule on the first two height functions. This curve can be seen in the third row of Figure 8. We can easily see that such a curve will envelop non-zero volume only under the third height function. We numerically simulated such a gait and indeed we obtain a motion of the kinematic snake which after one complete cycle only rotates the robot. All fiber motions are plotted in the last row of the third column of Figure 8.

Similarly we can design two other gaits, G_1^{KS} and G_2^{KS}, shown in (39) and (40), respectively, that result in moving the robot only in the x and y directions as shown in the f irst and second rows of Figure 8:

$$G_1^{\text{KS}}: \quad \begin{aligned} \sigma_1 &= \frac{\pi}{2} - 0.63778\cos(t) - 0.832148\sin(t), \\ \sigma_2 &= \frac{\pi}{2} - 1.01344\cos(t) + 0.268663\sin(t), \end{aligned} \tag{39}$$

Downloaded from ijr.sagepub.com at PENNSYLVANIA STATE UNIV on May 16, 2016

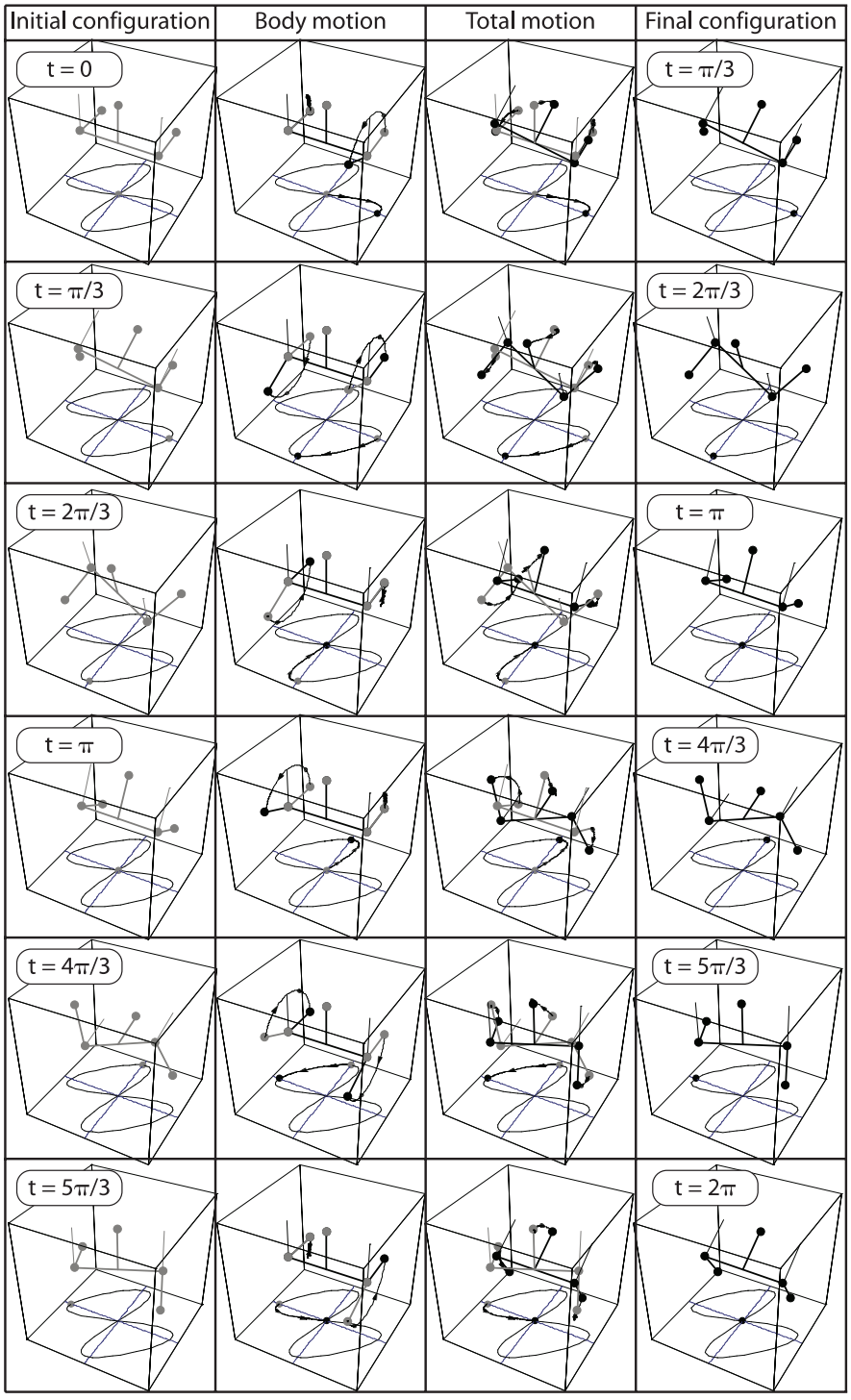

Fig. 6. This figure depicts the detailed motion of the pivoting dynamic model while performing the gait, G_1^{PDM}. The first column shows the robots initial conf iguration (shown in gray). The second column shows the body motion, that is, the internal shape motion. The starting shape is shown in gray while the final shapes are shown in black. The bottom of the plot depicts the actual motion in the base space along the gait, G_1^{PDM}. The third column depicts the actual motion of the robot that is due to the body motions. Finally, the last column depicts the final configuration of the robot after completing the interval of the gait. Note the net rotation, $\Delta\alpha$, about the x-axis between the top left and bottom right frames.

Downloaded from ijr.sagepub.com at PENNSYLVANIA STATE UNIV on May 16, 2016

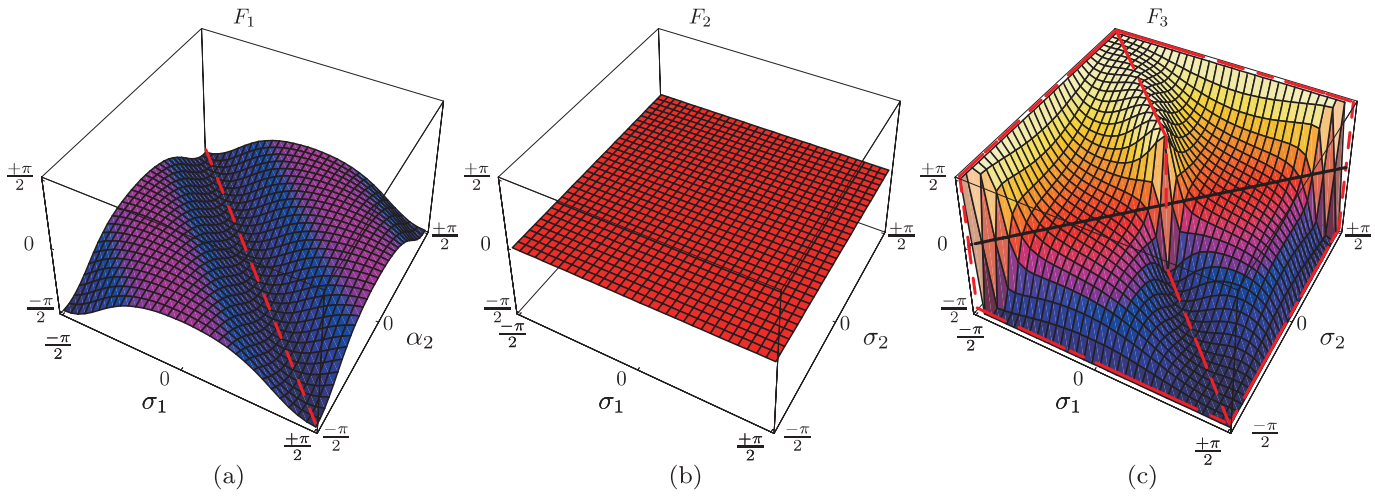

Fig. 7. The height functions corresponding to the three fiber directions expresses in body representation, $(\xi_x, \xi_y, \xi_\theta)$, for the kinematic snake robot. Darker colors of the height functions denote the negative regions while lighter colors denote the positive regions. We have used the arc-tangent function to bring the unbounded regions of the height function to $\pm\pi/2$. The dashed lines denote such unbounded regions where the robot has a singular configuration, while the solid lines indicate the zero lines. Note that the second height function is zero for all values of the base variables.

$$G_2^{\mathrm{KS}}: \quad \begin{aligned} \sigma_1 &= \frac{\pi}{2} + 1.03919\cos(t) - 0.139003\sin(t), \\ \sigma_2 &= \frac{\pi}{2} + 0.271378\cos(t) - 1.01271\sin(t), \end{aligned} \tag{40}$$

$$G_3^{\mathrm{KS}}: \quad \begin{aligned} \sigma_1 &= \frac{\pi}{4}(2 + [\pi(9\sin(4.1594 + 2t) \\ &+ 4\sin(2.0797 + t))][18\sqrt{2}]^{-1}), \\ \sigma_2 &= \frac{\pi}{4}(2 + [\pi(9\sin(4.1594 + 2t) \\ &- 4\sin(2.0797 + t))][18\sqrt{2}]^{-1}). \end{aligned} \tag{41}$$

Note that both gaits G_1^{KS} and G_2^{KS} have an identical base space curve, but different initial shapes. The initial shape is denoted by the solid dot in Figure 8. Moreover, in Figure 9, we plotted both the initial and final configurations of the kinematic snake for the three gaits we presented above. Finally, to understand the motion of the kinematic snake throughout a gait, we divided the entire motion of G_3^{KS} into smaller intervals and depicted both the body motion and total motion as shown in Figure 10.

9. Body versus Global Coordinates

Recall that we are computing all of the position change of the robot in a body-attached coordinate frame. In general, a change in position in a body-attached frame does not necessarily correspond to a direct global motion. In fact, the only case when a motion in body coordinates corresponds to identical motion in global coordinates is when the lifted group action is trivial, that is, in matrix form the map $T_g L_{g^{-1}}$ is the identity matrix. This was the case for the rolling disk example studied by Mukherjee and Anderson (1993).

This is not the case for either of the example systems we are analyzing in this paper. This can be clearly seen in the non-trivial lifted action maps depicted in (13) and (16), respectively. Hence, one should not expect that a non-zero motion along either ω_α or ξ_1 will directly correspond to a non-zero rotation about the x-axis for the pivoting dynamic model of a translation along the x-axis for the kinematic snake.

In fact, for the kinematic snake, after the elliptical gait to move the snake along the x and y, we ran a numerical simulation where we varied the initial shape of the snake. The gaits we simulated are given by

$$\begin{aligned} \sigma_1 &= \frac{\pi^2}{2\sqrt{2}}\left(+\frac{\sin(t+i)}{7} + \frac{\cos(t+i)}{4}\right) + \frac{1}{2}, \\ \sigma_2 &= \frac{\pi^2}{2\sqrt{2}}\left(-\frac{\sin(t+i)}{7} + \frac{\cos(t+i)}{4}\right) + \frac{1}{2}. \end{aligned}$$

By varying the variable i, we change the initial shape of the kinematic snake. Then we numerically simulate the gaits and compute the global position and orientation change. The results are depicted in Figure 11. Then we picked the two gaits for which the global motion was purely along either the x or y directions. The gaits we presented earlier were for $i = 2.81$ and 0.72 rad. Another interesting observation is the

Downloaded from ijr.sagepub.com at PENNSYLVANIA STATE UNIV on May 16, 2016

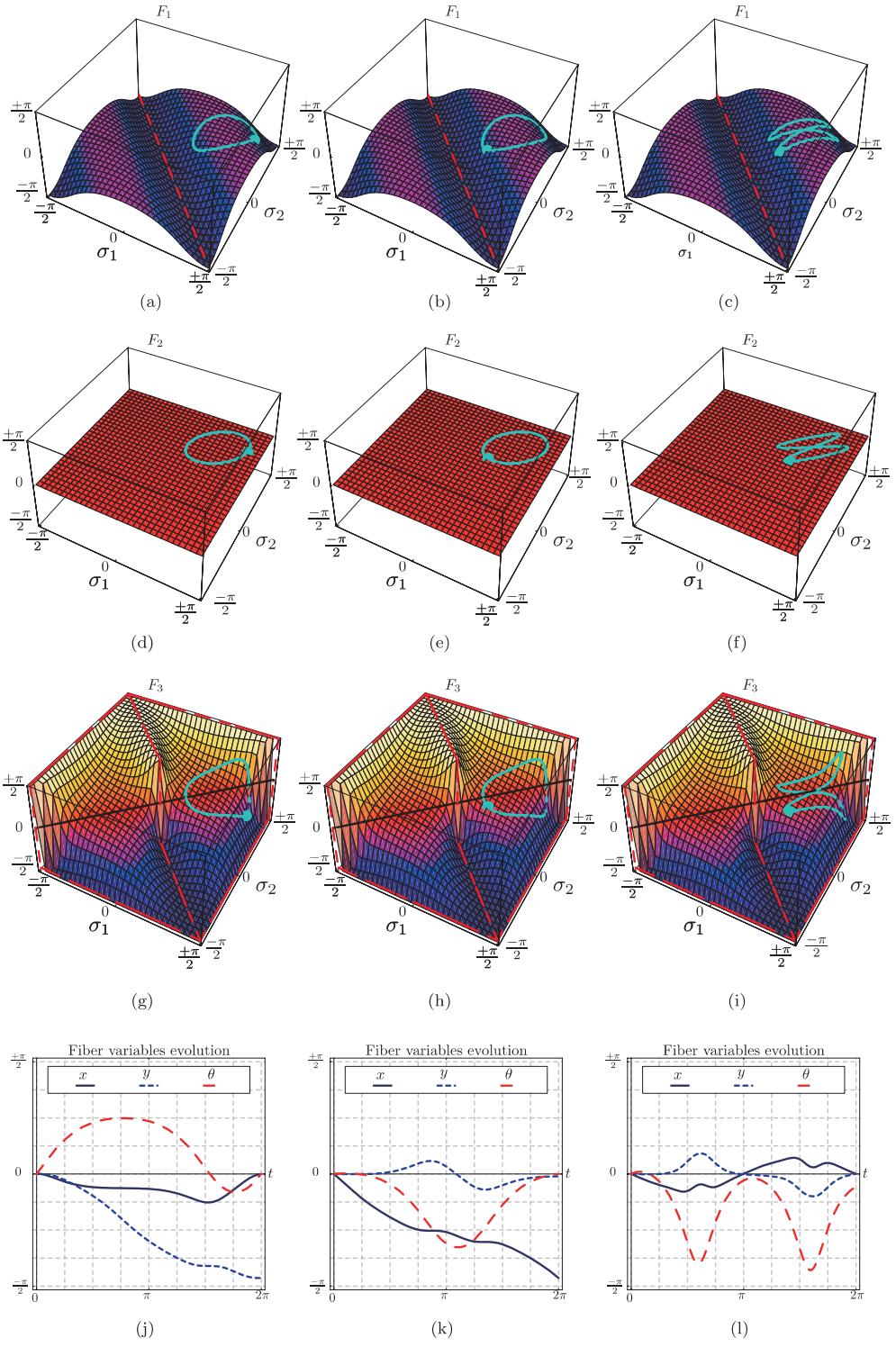

Fig. 8. Three sample gaits, $(G_1^{KS}, G_2^{\mathrm{KS}}, G_3^{\mathrm{KS}})$, that were designed to move the kinematic snake independently along each of the three fiber directions. The first two columns depict two gaits that move the robot along the x and y axes, respectively, while the third column depicts a gait that rotates the robot in the θ direction. Note that the solid dots on the gait curves in the first three rows indicate the initial shape of the kinematic snake for each of the gaits. The last row of each column depicts a time simulation of each gait where the fiber motions are plotted versus time.

Downloaded from ijr.sagepub.com at PENNSYLVANIA STATE UNIV on May 16, 2016

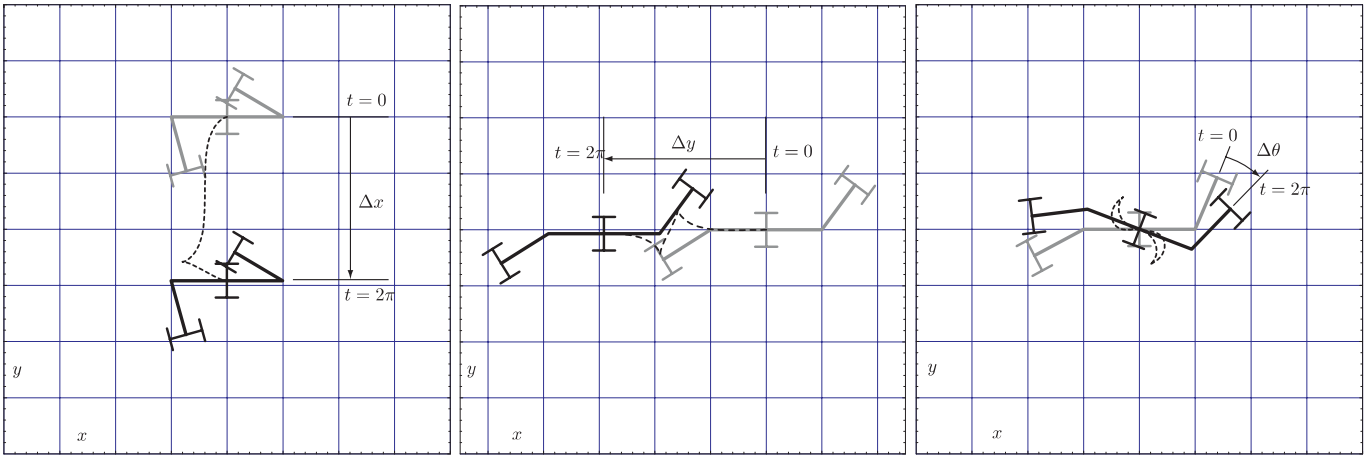

(a) (b) (c)

Fig. 9. Snapshots of the kinematic snake at the beginning (gray) and the end (black) of each period of the simulated gait, G_1^{KS}, G_2^{KS} and G_3^{KS}. Note the independent fiber motions, Δx, Δy and $\Delta\theta$, respectively. The light dashed lines denote the trace of the center of the middle link throughout the gait.

fact that the following function of the global position changes, $\sqrt{(\Delta x)^2 + (\Delta y)^2}$, is always constant and it is independent of the initial shape of the kinematic snake. This fact is shown in Figure 11.

10. Demonstrations

To demonstrate our gait generation techniques, we built two simple robots using Lego® blocks and hobby servos. Rather than building an actual pivoting dynamic model, we opted for a simpler *planar* version shown in Figure 12(a) as it was much easier to construct and still demonstrated our techniques. For this particular robot, the planar pivoting dynamic model, the configuration space is $q = (\theta, \sigma_1, \sigma_2) \in Q = \mathrm{SO}(2) \times \mathbb{S} \times \mathbb{S}$. This planar model has four concentrated masses. Then we computed the reduced mass matrix from which we can compute the mechanical connection.

Specifically for this robot, because the fiber space SO(2) is commutative, we can directly compute the change in the inertial angle, θ. Then integrating the connection we obtain

$$\begin{aligned}\Delta\theta &= \frac{HR^2}{2}\iint [R(\sin(\sigma_1) + \sin(\sigma_2)) \\ &- H\sin(\sigma_1 - \sigma_2)][(2H^2 + R^2 + HR(\cos(\sigma_1) \\ &- \cos(\sigma_2)))^2]\, d\sigma_1\, d\sigma_2\end{aligned}$$

A plot of the above height function, the integrand, is shown in Figure 12(b). Now consider the following base space curve:

$$G_1^{\mathrm{PPDM}}: \quad \begin{aligned}\sigma_1 &= \frac{\pi}{2}\left(1 + \cos(t)^{\frac{1}{5}}\right), \\ \sigma_2 &= \frac{\pi}{2}\left(1 + \sin(t)^{\frac{1}{5}}\right).\end{aligned}$$

This particular curve, G_1^{PPDM}, encloses a large volume and remains in the same positive region as shown in Figure 12(b). We have simulated this specific gait and plotted the change in the fiber angle, θ, versus time as shown in Figure 12(c). Finally, we plotted several snapshots of the planar pivoting model at the beginning and end of specific intervals of the square gait as shown in Figure 13. We have implemented this gait on our actual planar pivoting robot and indeed, as expected, the robot started to rotate after each cycle as shown in Figure 14. Nonetheless, the magnitudes of rotation of the actual robot did not match that of our model. The reasons for this mismatch we believe are due to the friction in the bearings around which the robot pivots and the slight errors in computing the mass and inertia of the actual links. We encourage the readers to check the videos in Extension 1 to better understand Figure 14.

As for the kinematic snake example, we constructed a similar robot to that we studied in this paper. In this case we applied two sinusoidal gaits. The first gait we applied was similar in structure to G_1^{KS}, that is, the gait was an elliptical non-intersecting gait that is symmetric with respect to the line $\sigma_1 = \sigma_2$. As expected, implementing this gait moved the kinematic snake along the same direction after each complete cycle. Snapshots of the actual robot are shown in Figure 15.

We would like to note that we observed some sideways slipping of the wheels and the magnitude of the slipping was more

Downloaded from ijr.sagepub.com at PENNSYLVANIA STATE UNIV on May 16, 2016

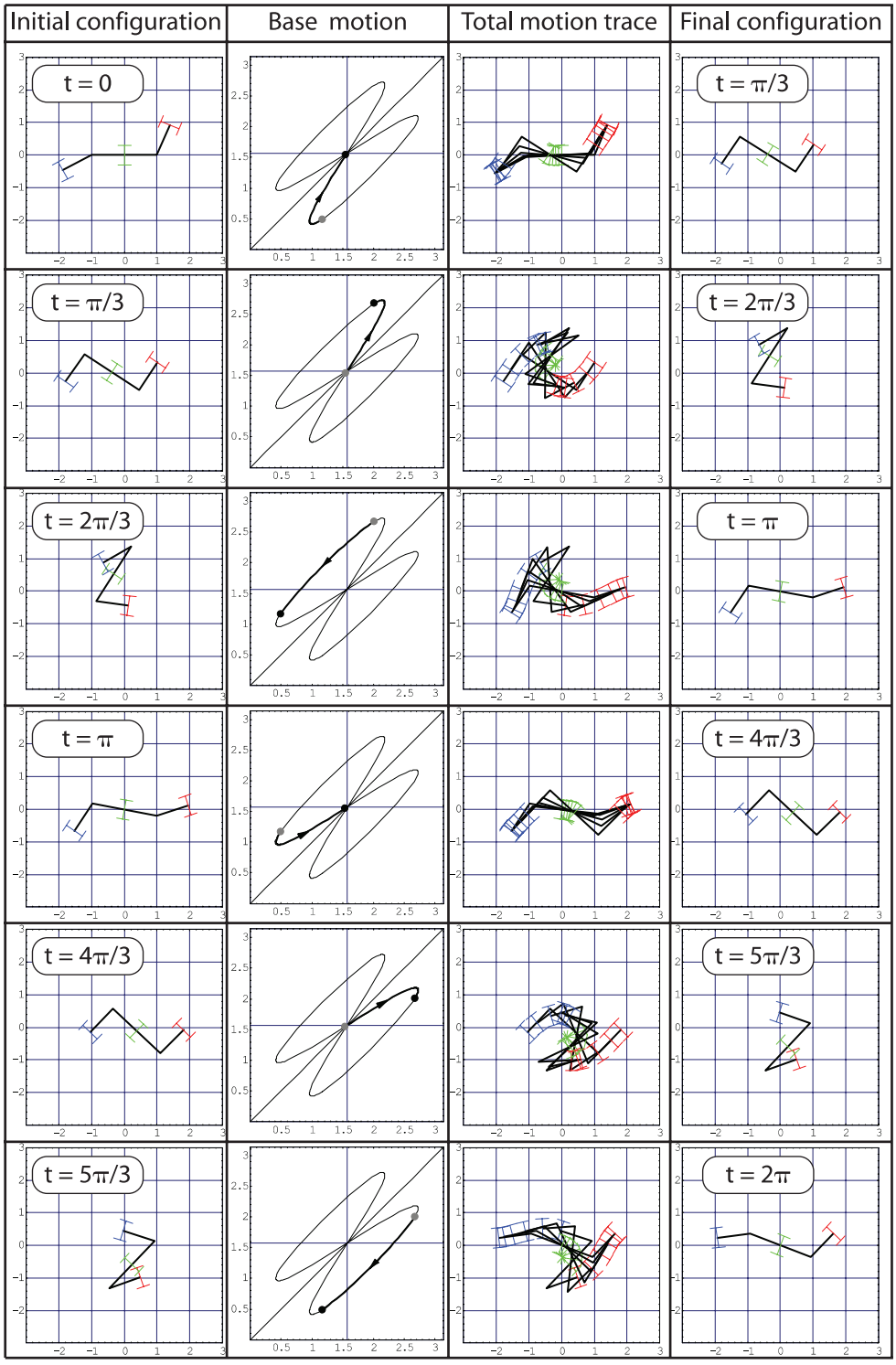

Fig. 10. Detailed motion of the kinematic snake while performing the gait, G_3^{KS}. The first column shows the robots initial configuration. The second column shows the body motion, that is, the internal shape motion. The gray dots depict the starting shape while the black dots depict the final shape. The third column depicts a trace of the actual motion of the robot that is due to the body motions. Finally, the last column depicts the final conf iguration of the robot after completing an interval of the gait. Note the net rotation, $\Delta\theta$, of the kinematic snake between the top left and bottom right frames.

Downloaded from ijr.sagepub.com at PENNSYLVANIA STATE UNIV on May 16, 2016

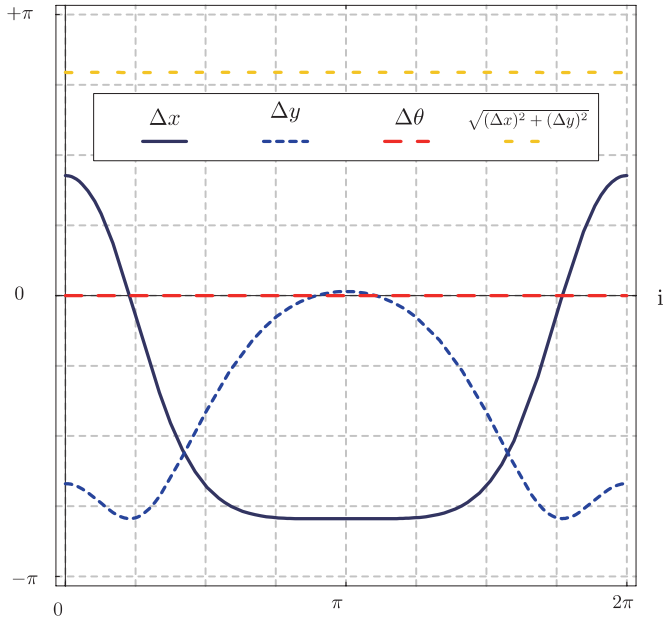

Fig. 11. The change in correspondence between body and global coordinate as a function of initial shape.

significant as our gaits approached the line $\sigma_1 = -\sigma_2$. This observation does match our intuition, because we know from our height function analysis that the line $\sigma_1 = -\sigma_2$ represents the singular conf igurations of the robot. Hence, according to our analysis, as the gaits approach the line $\sigma_1 = -\sigma_2$ they should envelop larger volumes, that is, the magnitudes of motion should increase. Moreover, we know that as the gaits approach the singular line $\sigma_1 = -\sigma_2$, the constraint forces increase in magnitude. Nonetheless, because the wheels on our kinematic snake robots are not ideal, as the constraint forces became larger and overcame the sideways frictional forces, the wheels started slipping. So, for gaits that approached the singular line $\sigma_1 = -\sigma_2$, rather than attaining larger magnitudes of motion, we observed some wheel slipping.

In fact, we pushed this idea to an extreme where we implemented a circular gait that was centered at the origin of the base space, that is, the gait actually crosses the singular line $\sigma_1 = -\sigma_2$ twice per cycle. Even though we observed considerable slipping of the wheels each time the gait passed through the singular line, the actual magnitude of motion along the x direction was relatively large when compared with the gaits we implemented earlier as shown in Figure 16. This is not an indication of a failure of our gait generation analysis which predicts infinite motion for such a gait, rather the actual model violated the non-holonomic constraints at these singular configuration and, due to slipping and modeling errors, produced a large finite motion. Finally, we implemented a figure-eight type curve which, as expected, rotated the kinematic snake in place as shown in Figure 17.

We encourage the readers to check the videos in Extension 1 to better understand Figures 15–17.

11. Higher-dimensional Base Spaces

The gait generation approach we have presented so far was intuitive and graphically elegant since the base space has been two-dimensional. Nonetheless, this approach is still valid in higher dimensional base spaces, but generating gaits is more tedious.

For example, consider the planer pivoting dynamic model shown in Figure 12(a) which is a purely mechanical system. Adding one more actuated link to one of the distal arms makes the base space three-dimensional, $m = 3$. For this specific system, the change in orientation, $\Delta\theta$, given in (34) will be equal to the sum of three volume integrals under three height functions, such that

$$\Delta\theta = \iint f_1(r)\, dr_1\, dr_2 + \iint f_2(r)\, dr_2\, dr_3 + \iint f_3(r)\, dr_1\, dr_3.$$

Thus, to generate gaits one should simultaneously analyze the three height functions for each fiber direction. Moreover, note that the height functions are three-dimensional, thus, the zero level sets that separate the signed regions are two-surfaces rather than one-dimensional curves as shown in Figures 3 and 7. In fact, we have solved for the integrand functions and we solved for the volumes in the base space where all three integrand functions are either positive or negative. These same-signed regions are depicted in Figure 18.

Note that Stokes' theorem is still valid, where we are transforming the integral of a one-form along a one-dimensional curve to an integral of a two-form over a two-surface which is implicitly defined. In fact, we have generated a gait that stayed within the positive region of all of the integrand functions. This gait is depicted in Figure 19(a). We verified that all of the integrand functions are indeed positive as shown in Figure 19(b). Finally, we simulated this proposed gait and, as expected, the four-link pivoting dynamic model does change its global orientation after the completion of the gaits, as shown in Figure 19(c).

As for the principally kinematic system we consider in this paper, the kinematic snake, adding an additional link will change the type of the system. An extra link will make the base space three-dimensional, but the extra set of wheels will add one more non-holonomic constraint. Thus, the system is not principally kinematic because we have one more non-holonomic constraint than the dimension of the fiber space, SE(2), which is three-dimensional. We argue that this additional link is unnecessary because using only three links and a two-dimensional base space is enough to fully span the fiber

Downloaded from ijr.sagepub.com at PENNSYLVANIA STATE UNIV on May 16, 2016

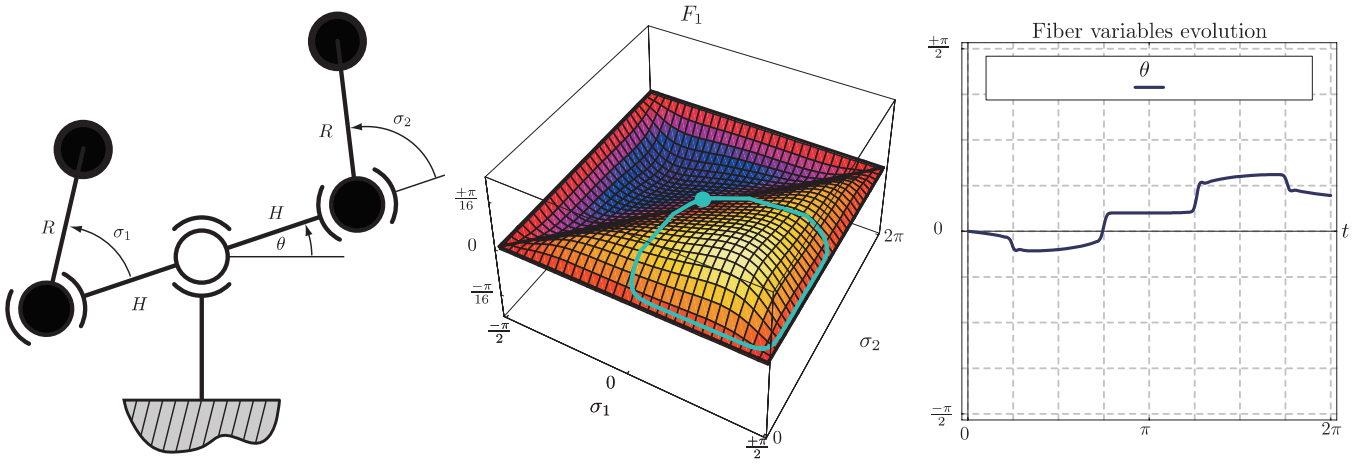

(a) (b) (c)

Fig. 12. (a) A schematic of the *planar* pivoting dynamic model denoting its configuration variables: (θ) is the fiber variable denoting the global orientation of the robot while (σ_1, σ_2) are the base variables denoting the rotations of the robot's arms. (b) The height function of the planar pivoting dynamic model with a simulated square gait. (c) The time simulation of the fiber angle, θ, for the simulated square gait.

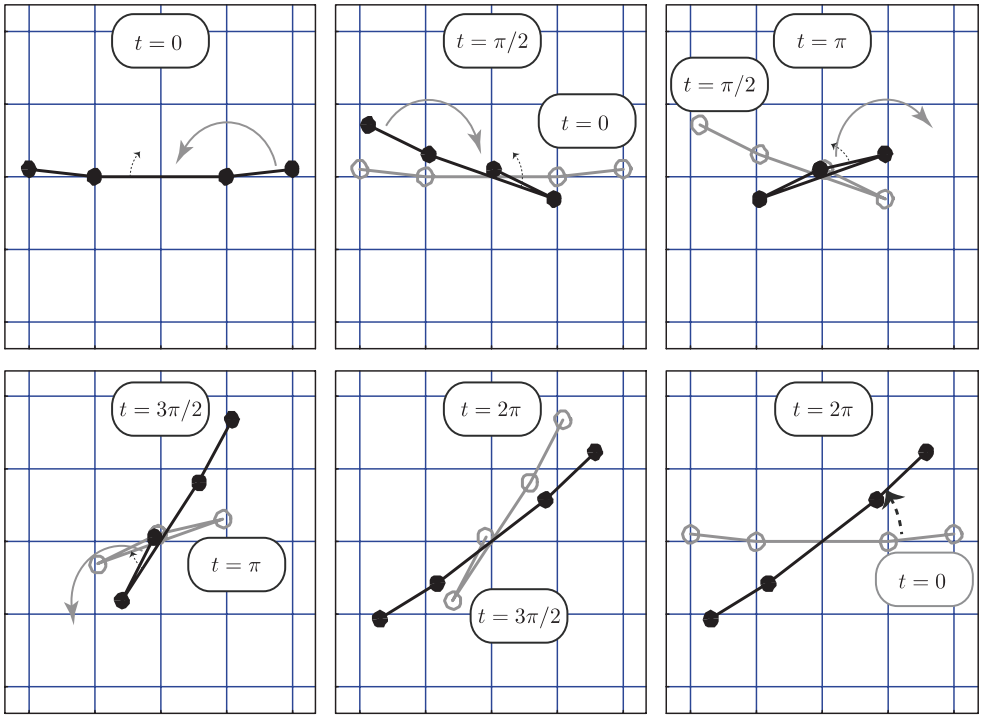

Fig. 13. Several snapshots of the robot throughout the gait. The big solid arrows indicate the base motion while the smaller dashed arrows indicate the expected fiber motion. The initial configuration of the robot is shown in gray, while the robot's final configuration is shown in black. The final plot depicts both the initial and final configuration of the planar pivoting dynamic model after completing the entire gait.

Downloaded from ijr.sagepub.com at PENNSYLVANIA STATE UNIV on May 16, 2016

Fig. 14. Several snapshots of the actual planer pivoting dynamic model while performing the square gait, G_1^{PPDM}. The frames are chosen to depict one complete gait where τ is the gait's period. Note the slight overall clockwise rotation of the model. Refer to Extension 2 to watch the original video of this demonstration.

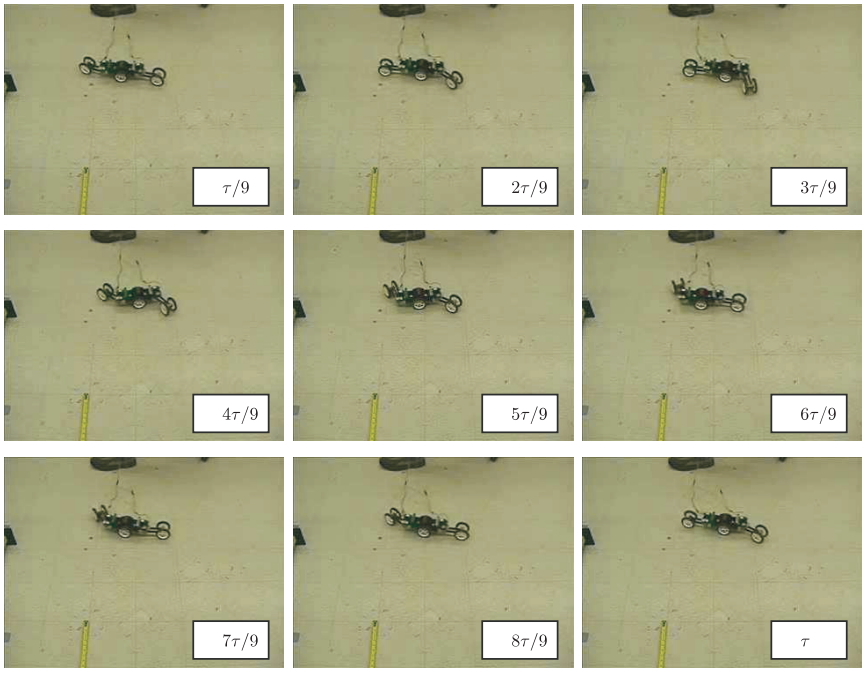

Fig. 15. Several snapshots of the actual kinematic snake while performing a figure-eight type curve. The frames are chosen to depict one complete gait where τ is the gait's period. Note the small translation of the robot in the x direction. Refer to Extension 2 to watch the original video of this demonstration.

Downloaded from ijr.sagepub.com at PENNSYLVANIA STATE UNIV on May 16, 2016

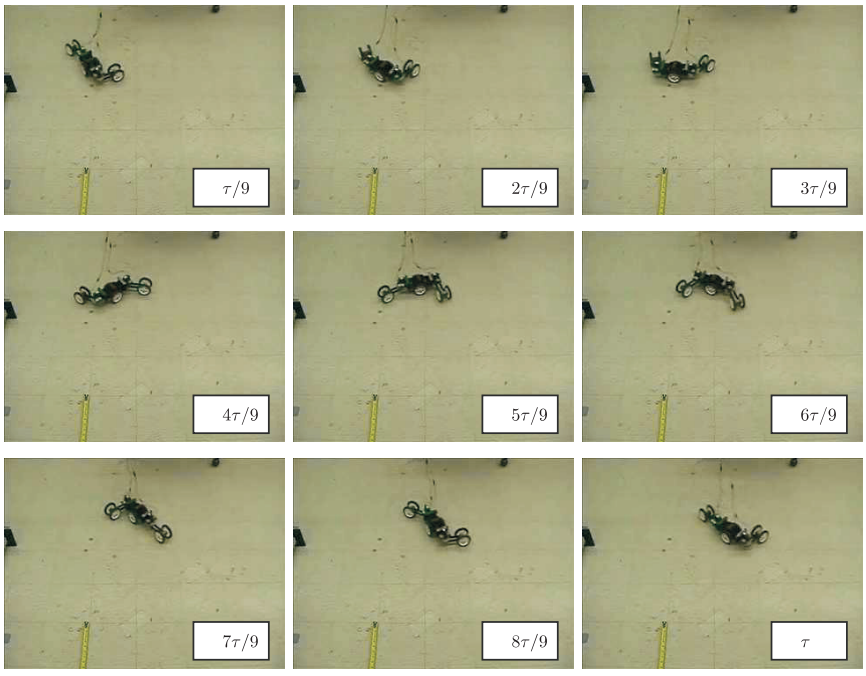

Fig. 16. Several snapshots of the actual kinematic snake while performing a *singular* figure-eight type curve. The frames are chosen to depict one complete gait where τ is the gait's period. Note the relatively large translation of the robot in the x direction. Refer to Extension 2 to watch the original video of this demonstration.

Fig. 17. Several snapshots of the actual kinematic snake while performing a *singular* figure-eight type curve. The frames are chosen to depict one complete gait where τ is the gait's period. Note the relatively large rotation of the kinematic snake. Refer to Extension 2 to watch the original video of this demonstration.

Downloaded from ijr.sagepub.com at PENNSYLVANIA STATE UNIV on May 16, 2016

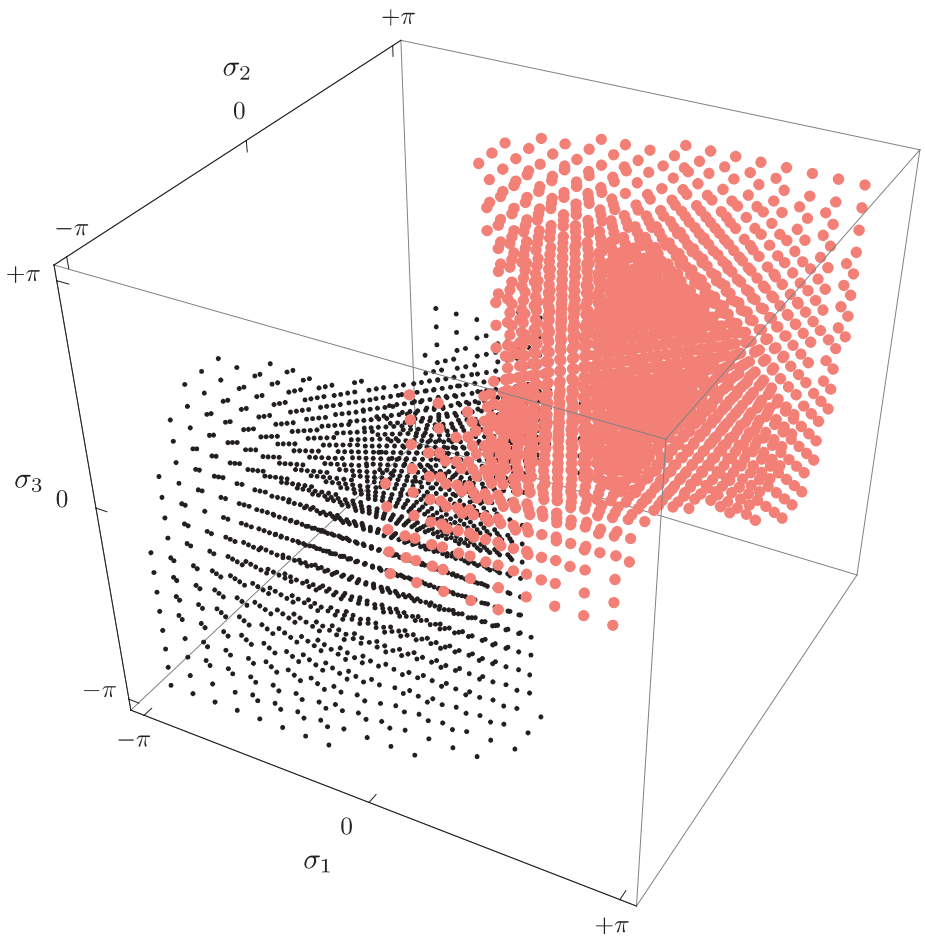

Fig. 18. For a planar four-link pivoting dynamic model, we depict the same-signed volumes where all three integrand function are either negative (black) or positive (gray).

space, that is, to locomote the kinematic snake in any direction. However, if an n-link kinematic snake is to be built, only three non-holonomic constraints should be linearly independent at any instant of time. This will keep the system purely kinematic and will provide enough equations to solve for the additional base variables to ensure the linear dependence of the additional non-holonomic constraints.

12. Conclusion and Future Work

In this paper, we have classified mechanical systems into three types and unified the gait generation analysis for two of them, the purely mechanical and principally kinematic systems. We related position change along the fiber direction to a volume integral. This simplified the gait evaluation problem which we then utilized to synthesize gaits by intuitively designing curves in the base space that produce the desired motions along a specified fiber variable represented in body coordinates. In addition, our technique adds no restriction on the shape of the gaits while also allowing us to depict all of the shape parameters of the suggested curves, which reduces the need for deeper intuition to manually or empirically setting these parameters.

Moreover, we identified two types of mechanical systems, purely mechanical and principally kinematic, whose reconstruction equations are structurally identical. This allowed us to use the same gait evaluation technique to generate geometric gaits for both systems. It is notable that we could use the same gait generation technique on two seemingly different systems whose motions are exclusively governed by two different types of constraints, momentum conservation laws or non-holonomic velocity constraints.

This paper constitutes our first step in solving the generic gait generation problem. Thus far we have analyzed mechanical systems whose reconstruction equation comprises solely a geometric term. Nonetheless, as we alluded to earlier in the

Downloaded from ijr.sagepub.com at PENNSYLVANIA STATE UNIV on May 16, 2016

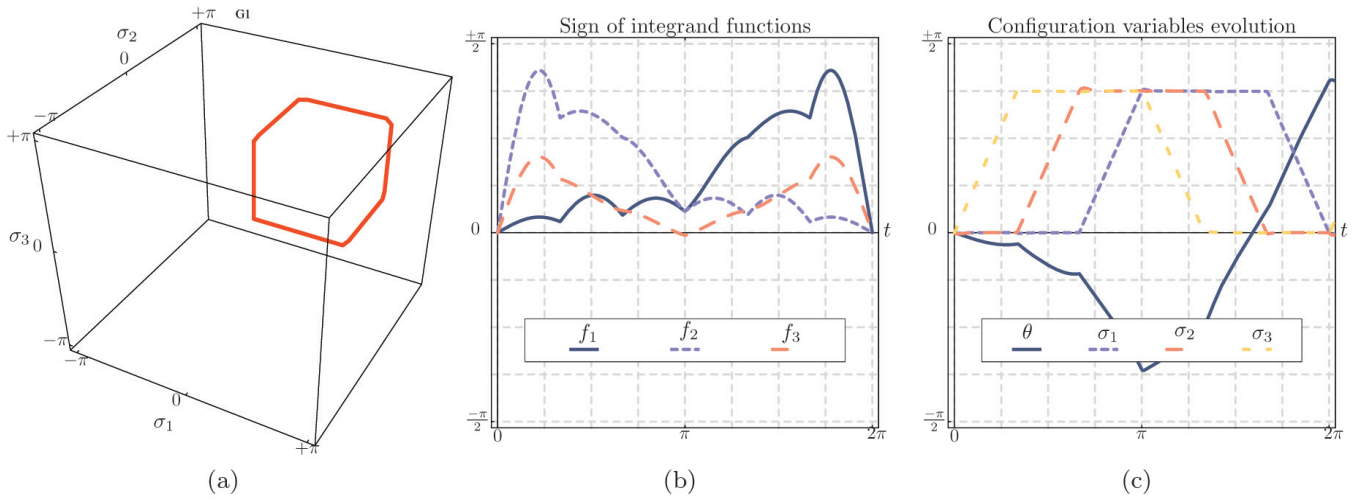

Fig. 19. (a) A proposed gait for the planar four-link pivoting dynamic model. (b) The values of the integrand function along the proposed gait. Note that all of the integrand functions are positive. (c) A time simulation of the proposed gait. Note the non-zero change in the global orientation of the planar four-link pivoting dynamic model.

paper, there exists a more general type of mechanical systems, namely mixed mechanical systems, where the reconstruction equation comprises two terms, the geometric term we analyzed in the paper and another dynamic term. This second dynamic term is dependent on the evolution of a generalized momentum of the mechanical system as well as the base space inputs.

In the companion paper (Shammas et al. 2007) we generalize the results presented in this paper to include mixed systems and we present how to generate gaits for such systems. In fact, we build upon our geometric gait analysis tools presented here and generate three types of gaits that locomote a mixed-type mechanical system using the geometric phase shift, the dynamic phase shift or both.

Finally, we would like to note that the analysis in this paper was performed in a body-attached coordinate frame. This representation has simplified our analysis at the cost of not directly controlling the global position change of the mechanical system. We acknowledge this fact of our gait analysis and we shall address this issue in our future work. Moreover, we want to emphasize that our gait analysis techniques presented in this paper do not provide optimal gaits as some of the prior work did; however, we believe that our analysis provides a space in which one can intuitively classify families of base space curves for gait generation.

Acknowledgments

We would like to thank Ravi Balasubramanian for allowing us to demonstrate our techniques on his pivoting dynamic model. We also would like to thank Anthony Kolb for helping in building the simple Lego robots and performing the locomotion experiments on them. Finally, we would like to thank the anonymous reviewers for their sincere and constructive inputs into this paper.

Appendix A: Background Material

Here we remind the reader of some of the basic concepts in Lagrangian mechanics and mechanics of locomotion. The readers are strongly encouraged to refer to Bloch et al. (2003, Chapters 1–5), Choset et al. (2000, Chapter 2), Cortés (2002, Chapters 2 and 3) and Marsden and Ratiu (1994, Chapters 4, 7 and 9) for an extensive study of simple mechanical systems and the structure of their configuration spaces. Most of the material in this section can be found in more detail in the above texts.

A.1. Lagrangian Mechanics

A.1.1. Configuration Manifolds

A configuration uniquely specifies the location in two or three dimensions of each physical point of the mechanism or robot. For a robot comprising many rigid bodies, both position or *fiber* variables, which describe the robot's position with respect to an inertial frame, and shape or *base* variables, which describe the robot's internal degrees of freedom, are needed to specify the robot's configuration.

A general configuration manifold for mechanical systems is usually denoted by $Q = (G, M)$, where G is the Lie group

Downloaded from ijr.sagepub.com at PENNSYLVANIA STATE UNIV on May 16, 2016

specifying the position of the robot and M is the base space specifying the shape of the robot. For mechanical systems, the configuration manifold has a *fiber bundle* structure.

Definition 2. (Fiber bundle). A manifold Q with a base subspace M and a projection map $\pi : Q \to M$ is a fiber bundle if for every $r \in M$ there exists a neighborhood $U \subset M$ and $r \in U$ such that $\pi^{-1}(U)$ is homeomorphic to $G \times U$, where $G = \pi^{-1}(r)$, that is, locally, $Q \cong G \times M$. Here G is a fiber which is def ined as the pre-image of $r \in M$ under the map π.

If the fiber G has a group structure then Q is a *principal* fiber bundle, moreover, if $Q = G \times M$ globally, then Q is a *trivial* fiber bundle. As we are dealing with simple mechanical systems, we can decompose their conf iguration space into $Q = G \times M$ whose structure is a *trivial fiber bundle*. Typically, the configuration space G is n-dimensional where the fiber space G is l-dimensional and the base space M is m-dimensional.

A.1.2. Non-holonomic Constraints

Non-holonomic constraints are constraints that typically act on configuration velocities and are, by definition, not integrable. Such constraints are typically seen in mechanical systems with wheels or rolling elements. The assumption that wheels cannot slide sideways or slip while rolling gives rise to a set of non-holonomic constraints. Usually, for mechanical systems the non-holonomic set of k constraints can be written in a Pfaffian form

$$\omega(q) \cdot \dot{q} = 0, \tag{42}$$

where $\omega(q)$ is a $k \times n$ matrix describing the constraints and $\dot{q}$ represents an element in the tangent space of the n-dimensional configuration manifold Q.

A.1.3. Equations of Motion

For mechanical systems there exits a Lagrangian function, $L(q, \dot{q})$, that maps elements in the tangent space of the configuration manifold to the reals. Usually, the Lagrangian for mechanical systems are defined as the kinetic energy of the system minus its potential energy. For the purpose of this Appendix we assume that the mechanical systems do not have any potential energy. In the absence of constraints the equations of motion derived from the Euler–Lagrange equations are given by

$$\frac{d}{dt}\left(\frac{\partial L(q,\dot{q})}{\partial \dot{q}_i}\right) - \frac{\partial L(q,\dot{q})}{\partial q_i} = \tau_i \tag{43}$$

for all $i = 1, \ldots, n$ and τ_i are the generalized forces. For mechanical systems that are subject to non-holonomic constraints, the constraints forces are added as unknown Lagrange multipliers along the constraint directions. Then (43) becomes

$$\frac{d}{dt}\left(\frac{\partial L(q,\dot{q})}{\partial \dot{q}_i}\right) - \frac{\partial L(q,\dot{q})}{\partial q_i} + \lambda_j \omega_i^j(q) = \tau_i, \tag{44}$$

for all $j = 1, \ldots, k$, where k is the number of non-holonomic constraints acting on the mechanical system.

A.2. Actions and Connections

Now we introduce several maps that allow us to map the system dynamics to a body-attached coordinate frame.

A.2.1. Actions and Lifted Action

Given the principal fiber bundle structure of the configuration manifold of mechanical systems and the Lie group structure of the fiber space we can define an *action* on the configuration manifold using the *left and right translations* of the Lie group.

Definition 3. (Left translation (Bloch et al. 2003)). Let G be a Lie group. A *left translation*[4] is a map $L_g : G \to G$ given by $L_g(h) = gh$ where $g, h \in G$.

The left translation represents the translation of a robot located at h by the action g. For the complete configuration $Q = G \times M$, we define[5] the *left action* and its *lifted action*.

Definition 4. (Left action and lifted action (Bloch et al. 2003)) A left action of a Lie group G on a manifold Q is a map $\Phi : G \times Q \to Q$ such that:

- $\Phi(e, q) = q$, for all $q \in Q$, e is the identity element of Q;
- $\Phi(h, \Phi(g, q)) = \Phi(hg, q)$, for all $q, h \in G$ and $q \in Q$.

The lifted action is the linear map $T_q\Phi_g : T_qQ \to T_qQ$, acting on velocity vectors[6]. Note that for any matrix Lie group G, the tangent space at the Lie group identity T_eG is a Lie algebra.

A.2.2. Connections

Based on the notions above, the *connection*[7], which is a key concept in the theory of principal fiber bundles can be introduced after defining the vertical space.

4. This is a representation of how matrix group elements act on each other. As matrix multiplication is not commutative, we have a distinction between left and right translations.
5. Using group actions from above, we can define higher-order actions that act on the entire bundle space or its tangent space.
6. The right action can be defined analogously.
7. Not only do connections provide a relation between base and shape motions, they also provide a decoupled local form at the fiber identity which allows the dynamics of locomotion to be split.

Downloaded from ijr.sagepub.com at PENNSYLVANIA STATE UNIV on May 16, 2016

Definition 5. (Vertical space). Let $Q = G \times M$ be a configuration space and $\pi : Q \to M$ be a projection. The vertical space is $V_q Q = \mathrm{Ker}(T\pi)$, where $T\pi$ is the lifted action of π.

Definition 6. (Connection). A connection is a map that is used to assign a horizontal subspace, $H_q Q \subset T_q Q$, for each point $q \in Q$ such that $H_q Q$ depends smoothly on q and:

- $T_q Q = V_q Q \oplus H_q Q$;
- $T_q \Phi_g(H_q Q) = H_{gq} Q$;

where $V_q Q$ is the vertical space.

Note that the horizontal subspace is everywhere isomorphic to the tangent space of the base manifold M. The *horizontal lift* is the isomorphism which maps vectors in the tangent space of the base space to the corresponding lifted vectors in $H_q Q$. It determines the relationship between motion in the base and motion in the total space. Owing to this, the connection states how net robot motion is created by performing shape changes. The connection can also be represented as a mapping $\mathcal{A}(q) : T_q Q \to \mathfrak{g}$ with the Lie algebra $\mathfrak{g}$ of G. Here, $\mathcal{A}(q)$ is a Lie-algebra valued one-form. Before stating the properties of this connection form, the concept of the *exponential map* and the *infinitesimal generator* are introduced.

Definition 7. (Exponential Map). Let G be a matrix Lie group with corresponding Lie algebra $\mathfrak{g}$. The function $\exp(t\xi) \in G$ is called the matrix exponential map with $\xi \in \mathfrak{g}$ and $t \in \mathbb{R}$. In other words, the exponential map returns a new group element which belongs to the flow that is tangent to ξ after time t.

Definition 8. (Infinitesimal Generator). Suppose that $\Phi : G \times Q \to Q$ is an action. For $\xi \in \mathfrak{g}$, $\Phi^\xi : \mathbb{R} \times Q \to Q$ defined by $\Phi^\xi(t, x) = \Phi(\exp(t\xi), x)$ is an $\mathbb{R}$-action on Q. The vector field on Q defined by

$$\xi_Q(x) = \left.\frac{d}{dt}\right|_{t=0} \Phi(\exp(t\xi), x)$$

is called the infinitesimal generator of the action corresponding to ξ. In other words, the infinitesimal generator generates a left-invariant vector field over the entire manifold using the Lie algebra element ξ.

Now having defined the infinitesimal generator, we can state the properties of a *connection form* $\mathcal{A}(q) : T_q Q \to \mathfrak{g}$ (Bloch et al. 2003):

- $\mathcal{A}(q)\xi_Q = \xi \quad \text{for} \quad \xi \in \mathfrak{g}$;
- $\mathcal{A}(\Phi_g q) T_q \Phi_g \dot{q} = \mathrm{Ad}_g \mathcal{A}(g)\dot{q}$;

where $\mathrm{Ad}_g = T_g R_{g^{-1}} T_e L_g$.

A.2.3. Mechanical Connection

For mechanical systems, there is a natural definition of the connection. It involves the so-called *momentum map* J and the *locked inertia tensor* $\mathbb{I}$.

Definition 9. (Momentum Map). The momentum map is the map $J : TQ \to \mathfrak{g}^*$ with $\langle J(v_q); \xi \rangle = \langle\langle v_q, \xi_Q \rangle\rangle$ for all $\xi \in \mathfrak{g}$ and $v_q \in T_q Q$. Here $J(v_q)$ is the momentum of the system measured in spatial coordinates, $\langle v; \xi \rangle$ is the natural pairing between vector and co-vectors, $\langle\langle v_p, v_q \rangle\rangle = v_p^{\mathrm{T}} M v_q$ is the kinetic energy metric and M is the mass matrix.

Both terms, $\langle J(v_q); \xi \rangle$ and $\langle\langle v_q, \xi_Q \rangle\rangle$, are energy terms but are computed either using the momentum map or the kinetic energy metric, respectively.

Definition 10. [Locked inertia tensor] The locked inertia tensor is the map $\mathbb{I}(q) : \mathfrak{g} \to \mathfrak{g}^*$ which satisfies $\langle \mathbb{I}(q)\xi; \eta \rangle = \langle\langle \xi_Q, \eta_Q \rangle\rangle$ for all $\xi, \eta \in \mathfrak{g}$, where $\mathfrak{g}^*$ is the dual space to the Lie algebra $\mathfrak{g}$. Note that, $\mathbb{I}(q)$ is the inertia of the system with all base variables held fixed.

Considering the above definitions, the mechanical connection is given by

$$\mathcal{A}(q) = \mathbb{I}^{-1}(q) J. \tag{45}$$

As we are dealing with mechanical systems whose configuration space has a trivial fiber bundle structure, the connection can be written in a local trivialization.

Proposition 1. Let $\mathcal{A}$ be a connection form over a trivial fiber bundle[8]. Then $\mathcal{A}$ can be written as

$$\mathcal{A}(q)\dot{q} = \mathrm{Ad}_g(T_g L_{g^{-1}} \dot{g} + A(r)\dot{r}), \quad \text{for all} \quad q = (g, r) \in Q. \tag{46}$$

In this equation, $A(r)$ is called the *local* form of the connection. Note that the local form only depends on the base variables r. Rewriting the above equation in body coordinates simplifies it even further.

Definition 11. (Body representation velocity). Let $\dot{q} \in T_q Q$ be a configuration velocity at the point $q = (g, r)$ and let the body frame be attached to q. The body representation of $\dot{q}$ is $\xi^b = T_g L_{g^{-1}} \dot{g}$. In this paper, we use the body representation and, hence, ξ refers to ξ^b. As for the base velocity component, $\dot{r}$, it remains unchanged. The body velocity is the velocity of the origin of the body frame computed in the inertial frame but represented in the body frame (Murray et al. 1994).

8. This proposition can be seen in Bloch et al. (2003); however, it is proven for principal connections, but nonetheless still applies for mechanical connections on trivial principal fiber bundles.

Downloaded from ijr.sagepub.com at PENNSYLVANIA STATE UNIV on May 16, 2016

Using body representation we can define $\mathcal{A}^b(q)\dot{q} = \mathbb{I}^{-1}J^b$ where $\mathcal{A}^b(q) = \mathrm{Ad}_{g^{-1}}\mathcal{A}(q)$. Then rewriting (46) in body coordinates we obtain

$$\mathcal{A}^b(q)\dot{q} = \mathbb{I}^{-1}J^b = \xi + A(r)\dot{r},$$

or

$$\xi = -A(r)\dot{r} + \mathbb{I}^{-1}J^b. \tag{47}$$

This last equation is very important as it decouples the fiber velocities, ξ, and the base velocities, $\dot{r}$.

A.3. Invariance and Reduction

In this section we define invariance which allows us to compute the reduced Lagrangian and the reduced non-holonomic constraints.

A.3.1. Invariance

Invariance is a very powerful tool that is used in physics to exploit the symmetries in the formulation of a physical problem and, hence, remove "unnecessary variables". For example, the laws of physics are invariant with respect to translations, in other words, the placement of an inertial frame in which you do all your measurements is unimportant. Hence, we use invariance to reduce the order of the equations of motion of the mechanical systems we are studying. To remove the translational symmetries that arise from doing measurements in an inertial frame we map everything to a body attached reference frame. This allows us to rewrite the equations of motion in a reduced form.

A.3.2. Reduced Mass Matrix

To rewrite the dynamics in the body attached coordinate frame, we use the lifted actions defined earlier to define the body representation of a configuration velocity.

Moreover, the independence of the location of the inertial frame leads to the invariance[9]. of the Lagrangian, that is,

$$L((g^{-1}g, r), (T_gL_{g^{-1}}\dot{g}, \dot{r})) = L(q, \dot{q}). \tag{48}$$

This allows us to compute the *reduced Lagrangian*, $l(\xi, r, \dot{r})$, which according to Ostrowski (1995) will have the following form

$$l(\xi, r, \dot{r}) = \frac{1}{2}\begin{pmatrix}\xi & \dot{r}\end{pmatrix}^{\mathrm{T}}\tilde{M}\begin{pmatrix}\xi \\ \dot{r}\end{pmatrix} \tag{49}$$

or

$$\tilde{M} = \begin{pmatrix} I(r) & I(r)A(r) \\ A^{\mathrm{T}}(r)I^{\mathrm{T}}(r) & m(r)\end{pmatrix} \tag{50}$$

and where $\tilde{M}$ is the reduced mass matrix, $A(r)$ is the local form of the mechanical connection, $I(r)$ is the local form of the locked inertia tensor, that is, $I(r) = \mathbb{I}(e, r)$ (e is the Lie group identity element) and $m(r)$ is a matrix depending only on base variables. The reduced mass matrix is important, because we can solve for the mechanical connection, $A(r)$, simply by manipulating sub-matrices of the reduced mass matrix.

A.3.3. Reduced Non-holonomic Constraints

Given the triviality of the configuration space structure and the invariance of the constraints with respect to left group actions, we have

$$\omega(g, r)\cdot(\dot{g}, \dot{r})^{\mathrm{T}} = \omega(g^{-1}g, r)\cdot(T_gL_{g^{-1}}\dot{g}, \dot{r})^{\mathrm{T}}. \tag{51}$$

We know that $\xi = T_gL_{g^{-1}}\dot{g}$ and $e = g^{-1}g$, the group identity. Then ω must be only a function of the base variables. We label the sub-matrices of $\bar{\omega}(r)$ such as $\bar{\omega}(r) = (\bar{\omega}_\xi(r), \bar{\omega}_r(r))$, then the set of non-holonomic constraints can be written in the following reduced from

$$\bar{\omega}_\xi(r)\xi + \bar{\omega}_r(r)\dot{r} = 0. \tag{52}$$

The above equation is derived in Lemma B.1 in Appendix B.

A.4. Reduced Equations of Motion

Having verified that the Lagrangian and the non-holonomic constraints are invariant with respect to the Lie group actions we can go ahead and compute the reduced equations of motion.

A.4.1. Unconstrained Mechanical Systems

The equations of motion can be derived from the reduced Lagrangian. First we write out the original Euler–Lagrange equations using the reduced Lagrangian at the group identity, $g = e$. Then (43) becomes

$$\begin{aligned}\tau_i^g &= \frac{d}{dt}\left(\frac{\partial l}{\partial \dot{g}^i}\right) - \frac{\partial l}{\partial g^i} \\ &= \frac{d}{dt}\left(T_gL_{g^{-1}}\frac{\partial l}{\partial \xi^i}\right) - \frac{T_gL_{g^{-1}}\dot{g}}{g^i}\frac{\partial l}{\partial \xi^i} \qquad (53)\\ \tau_i^r &= \frac{d}{dt}\left(\frac{\partial l}{\partial \dot{r}^i}\right) - \frac{\partial l}{\partial r^i}, \qquad (54)\end{aligned}$$

9. Invariance allows us to compute the Lagrangian anywhere along the fiber space, the group identity was chosen in particular.

Downloaded from ijr.sagepub.com at PENNSYLVANIA STATE UNIV on May 16, 2016

where we used $\xi = T_g L_{g^{-1}} \dot{g}$.

Defining the generalized momentum as $p = \frac{\partial l}{\partial \xi}$, the above equations of motion and local trivialization of the mechanical connection in (47) become

$$\dot{p}_i - \mathrm{ad}^*_\xi p_i = \tau_i^e \tag{55}$$

$$\frac{d}{dt}\left(\frac{\partial l}{\partial \dot{r}^i}\right) - \frac{\partial l}{\partial r^i} = \tau_i^r \tag{56}$$

$$\xi = T_g L_{g^{-1}} \dot{g} = -A(r)\dot{r} + I^{-1}(r) p^{\mathrm{T}}, \tag{57}$$

where τ^e is the forcing function in the group directions pulled back to the group identity (for the reduced form of the Lagrangian). The first equation represents the momentum equation with the momentum p and the second equation constitutes the dynamic equations for the base space. Having solved for the base and momentum variables, the group motion is computed by (57), which is often referred to as the *reconstruction* equation (Kelly 1998; Ostrowski 1995).

Hence, using invariance we were able to rewrite the n $(= l + m)$ second-order differential equations of motion in (43) as a set of $2l$ first-order differential equation in (55) and (57) and m second-order differential equations in (56).

A.5. Exterior Algebra

Finally, we conclude with a result from exterior algebra theory. We review Stokes' theorem in its most general form.

Theorem 1. (Stokes' Theorem) *Given a one-form ω and its exterior derivative $d\omega$, we have*

$$\oint_{\partial N} \omega = \int_N d\omega, \tag{58}$$

where ∂N is the boundary of the manifold N.

The exterior derivative of a one-form, $\omega = \sum_{i=1}^m f_i(\sigma_1, \sigma_2, \cdots, \sigma_m) d\sigma_i$, yields a two-form and is given by

$$d\omega = \sum_{i,j=1, i<j}^{m} \left(\frac{\partial f_j}{\partial \sigma_i} - \frac{\partial f_i}{\partial \sigma_j}\right)(d\sigma_i \wedge d\sigma_j),$$

where $\wedge$ represents the wedge product (Darling 1994; Lugo 1998).

Appendix B

Here we state and prove Lemma B.1.

Lemma 1. Suppose that we are given a mechanical system whose configuration space is a trivial principal bundle $Q^n = G^l \times M^m$, that is, $q = (g, r) \in Q$ and $\dot{q} = (\dot{g}, \dot{r}) \in T_q Q$. Moreover, let the system be subject to k linearly independent non-holonomic constraints $\omega(q) \cdot \dot{q} = 0$ that are invariant with respect to left group actions. Then we have

$$T_g L_{g^{-1}} \dot{g} = -\mathbb{A}(r)\dot{r},$$

where $T_g L_{g^{-1}} \dot{g}$ is the body representation of a fiber velocity $\dot{g}$, $\mathbb{A}(r)$ is a $l \times m$ matrix that is referred to as the local form of the principally kinematic connection and $\dot{r}$ is a shape space velocity.

Proof. Given the triviality of the configuration space and the invariance of the constraints with respect to left group actions, we have

$$\omega(q) \cdot \dot{q} = \omega(\Phi_h q) \cdot T_q \Phi_h \dot{q},$$

or

$$\omega(g, r) \cdot (\dot{g}, \dot{r})^{\mathrm{T}} = \omega(L_h g, r) \cdot (T_g L_h \dot{g}, \dot{r})^{\mathrm{T}},$$

where $\Phi_h q$ and $T_q \Phi_h \dot{q}$ are the left and lifted left actions on the manifold Q (Bloch et al. 2003; Ostrowski and Burdick 1998). Note that these actions act only on the fiber part of q. Let $h = g^{-1}$ and using (42) we have

$$\begin{aligned} 0 = \omega(g, r) \cdot (\dot{g}, \dot{r})^{\mathrm{T}} &= \omega(L_{g^{-1}} g, r) \cdot (T_g L_{g^{-1}} \dot{g}, \dot{r})^{\mathrm{T}} \\ &= \omega(g^{-1} g, r) \cdot (T_g L_{g^{-1}} \dot{g}, \dot{r})^{\mathrm{T}} \\ &= \bar{\omega}(r) \cdot (T_g L_{g^{-1}} \dot{g}, \dot{r})^{\mathrm{T}}. \end{aligned}$$

Let $\xi = T_g L_{g^{-1}} \dot{g}$ and $\bar{\omega}(r) = (\bar{\omega}_1(r), \bar{\omega}_2(r))$, then writing the above equation in matrix form we obtain

$$\begin{pmatrix} \bar{\omega}_1(r) & \bar{\omega}_2(r) \end{pmatrix} \cdot \begin{pmatrix} \xi \\ \dot{r} \end{pmatrix} = 0.$$

Solving for ξ we get

$$\xi = T_g L_{g^{-1}} \dot{g} = \overbrace{(\bar{\omega}_1(r))^{-1} \cdot \bar{\omega}_2(r)}^{-\mathbb{A}(r)} \cdot \dot{r}.$$

The fact that the non-holonomic constraints are linearly independent implies that $\bar{\omega}_1(r)$ is invertible. Also note that $\mathbb{A}(r)$ depends only on the base variables. ■

Downloaded from ijr.sagepub.com at PENNSYLVANIA STATE UNIV on May 16, 2016

Appendix C: Index to Multimedia Extensions

Table of Multimedia Extensions.

Extension	Type	Description
1	Code	Mathematica® code where most of the figures of this paper were generated. This code will allow the user to rework the examples we introduced in this paper and analyze other mechanical systems. The readers can install Mathematica® Player to read the code if they do not have access to Mathematica®.
2	Video	Demonstration videos from which Figures 14–17 are extracted from.

The multimedia extension page is found at http://www.ijrr.org

References

Balasubramanian, R. and Rizzi, A. A. (2004). Kinematic reduction and planning using symmetry for a variable inertia mechanical system. *Proceedings of the IEEE/RSJ International Conference on Intelligent Robots and Systems*, vol. 4, September, pp. 3829–3834.

Balasubramanian, R., Rizzi, A. A. and Mason, M. T. (2003). Legless locomotion for legged robots. *Proceedings of the IEEE/RSJ International Conference on Robotics and Intelligent Systems*, vol. 1, October, pp. 880–885.

Bloch, A., Baillieul, J., Crouch, P. E. and Marsden, J. E. (2003). *Nonholonomic Mechanics and Control*. Berlin, Springer.

Brockett, R. W. (1981) Control theory and singular Riemanian geometry. *New Directions in Applied Mathematics*, Hilton, P. J. and Young, G. S. (eds). New York, Springer, pp. 11–27.

Brockett, R. W. and Dai, L. (1993). Nonholonomic kinematics and the role of elliptic functions in constructive controllability. *Nonholonoimc Motion Planning*, Li, Z. and Canny, J. F. (eds). New York, Kluwer, pp. 1–21.

Chitta, S., Heger, F. and Kumar, V. (2004) Dynamics and gait control of a rollerblading robot. *Proceedings of the IEEE International Conference on Robotics and Automation*, vol. 4, May, pp. 3944–3949.

Chitta, S., Cheng, P., Frazzoli, E. and Kumar, V. (2005). RoboTrikke: a novel undulatory locomotion system. *Proceedings of the IEEE International Conference on Robotics and Automation*, April, pp. 1597–1602.

Choset, H., Luntz, J., Shammas, E., Rached, T., Hull, D. and Dent, C. (2000). Design and motion planning for serpentine robots. *Proceedings of the Tokyo Institute of Technology Super Mechano Systems Workshop*, Tokyo, Japan.

Choset, H., Lynch, K. M., Hutchinson, S., Kantor, G., Burgard, W., Kavraki, L. E. and Thrun, S. (2005). *Principles of Robot Motion: Theory, Algorithms, and Implementations*. Cambridge, MA, MIT Press.

Cortés, J. (2002). *Geometric, Control and Numerical Aspects of Nonholonomic Systems*. New York, Springer.

Darling, R. W. R. (1994). *Differential Forms and Connections*. Cambridge, Cambridge University Press.

Hirose, S. (1993). *Biologically Inspired Robots (Snake-like Locomotor and Manipulator)*. Oxford, Oxford University Press.

Kelly, S. (1998). The mechanics and control of robotic locomotion with applications to aquatic vehicles. *Ph.D. Thesis*, California Institute of Technology.

Lugo, G. (1998). Differential geometry in physics. *Technical Report*, University of North Carolina.

Marsden, J. E. and Ratiu, T. S. (1994). *Introduction to Mechanics and Symmetry*. Berlin, Springer.

Mukherjee, R. and Anderson, D. P. (1993). Nonholonomic motion planning using Stoke's theorem. *Proceedings of the IEEE International Conference on Robotics and Automation*, vol. 3, May, pp. 802–809.

Murray, R. M. and Sastry, S. S. (1993). Nonholonomic motion planning: steering using sinusoids. *IEEE Transactions on Automatic Control*, **38**(5): 700–716.

Murray, R. M., Li, Z. and Sastry, S. S. (1994). *A Mathematical Introduction to Robotic Manipulation*. Boca Raton, FL, CRC Press.

Nakamura, Y. and Mukherjee, R. (1989). Nonholonomic path planning of space robots. *Proceedings of the IEEE International Conference on Robotics and Automation*, vol. 2, May, pp. 1050–1055.

Nakamura, Y. and Mukherjee, R. (1991). Nonholonomic path planning of space robots via a bidirectional approach. *IEEE Transactions on Robotics and Autmation*, **7**: 500–514.

Ostrowski, J. (1995). The mechanics of control of undulatory robotic locomotion. *Ph.D. Thesis*, California Institute of Technology.

Ostrowski, J. and Burdick, J. W. (1998). The mechanics and control of undulatory locomotion. *International Journal of Robotics Research*, **17**(7): 683–701.

Ostrowski, J., Desai, J. and Kumar, V. (2000). Optimal gait selection for nonholonomic locomotion systems. *International Journal of Robotics Research*, **19**(3): 225–237.

Shammas, E., Choset, H. and Rizzi, A. A. (2005a). Natural gait generation techniques for principally kinematic mechanical systems. *Proceedings of Robotics: Science and Systems*, Cambridge, MA, June.

Shammas, E., Schmidt, K. and Choset, H. (2005b). Natural gait generation techniques for multi-bodied isolated mechanical systems. *Proccedings of the IEEE International*

Downloaded from ijr.sagepub.com at PENNSYLVANIA STATE UNIV on May 16, 2016

Conference on Robotics and Automation, April, pp. 3664–3669.

Shammas, E., Choset, H. and Rizzi, A. A. (2007). Towards a unified approach to motion planning for dynamic underactuated mechanical systems with non-holonomic constraints. *International Journal of Robotics Research*, **26**(10): 1075–1124.

Walsh, G. C. and Sastry, S. S. (1991). On reorienting linked rigid bodies using internal motions. *Proceedings of the 30th IEEE Conference on Decision and Control*, Brighton, December, pp. 1190–1195.

Walsh, G. C. and Sastry, S. S. (1995). On reorienting linked rigid bodies using internal motions. *IEEE Transactions on Robotics and Automation*, **11**(1): 139–146.

Yamada, K. (1993). Arm path planning for a space robot. *Proceedings of the IEEE/RSJ International Conference on Intelligent Robots and Systems*, vol. 3, July, pp. 2049–2055.

Downloaded from ijr.sagepub.com at PENNSYLVANIA STATE UNIV on May 16, 2016